UNIVERSIDAD AUTÓNOMA METROPOLITANA
UNIDAD AZCAPOTZALCO

Master thesis

Spatio-temporal simulation of intracellular Ca^{2+} dynamics during *Shigella* invasion

Author:

I.Q. Roberto Ornelas Guevara

Supervisor
Dra. Virginia González Vélez
Depto. Ciencias Básicas
UAM Azcapotzalco

Advisor
Dra. Geneviève Dupont
Unité de Chronobiologie Théorique
Université Libre de Bruxelles

June, 2019

Agradecimientos

Este trabajo no se pudo haber llevado a cabo sin el apoyo otorgado por el Consejo Nacional de Ciencia y Tecnología (CONACyT), tanto por la beca otorgada para llevar a cabo estudios de maestría como la beca de movilidad para la realización de una estancia de investigación en la Université Libre de Bruxelles (ULB) en Bruselas, Bélgica.

Agradezco a la Dra. Virginia González Vélez por la motivación y el apoyo para la realización de este proyecto.

Agradezco al Dr. Héctor Puebla por escucharme siempre que tuve dudas y por sus valiosos consejos.

I would like to thank Dr. Geneviève Dupont for allowing me to carry out the research stay at the ULB, as well as for her amiability, accurate observations and advice.

I would like to thank Dr. Benjamin Wacquier for the crucial support provided for the realization of this project since its beginning and during the stay at the ULB, which was more enjoyable and productive thanks to his friendship, observations and talks.

A mi familia y mis amigos.

Universidad Autónoma Metropolitana – Azcapotzalco

Abstract

UAM-A
División de Ciencias Básicas e Ingeniería

Master Degree in Process Engineering

Spatio-temporal simulation of Ca^{2+} dynamics during *Shigella* invasion

By

Roberto Ornelas Guevara

Shigellosis is an important problem of public health worldwide. It is mainly caused by the ingestion of food or water contaminated with *Shigella.* After its ingestion, this bacterium invades the colon and causes an intense inflammatory reaction, leading to destruction of the epithelial tissue. During invasion of the epithelial cells, *Shigella* induces atypical Ca^{2+} signals; however, it is not clear how these signals are generated or how to control them (Tran Van Nhieu *et al.*, 2013).

It is well known that cells use Ca^{2+} as a second messenger to control a wide array of cellular functions, including reorganisation of the cytoskeleton, inflammatory responses and cellular death (Sun *et al*., 2017). In this line, it has been reported that the perturbation of cellular Ca^{2+} homeostasis caused by *Shigella* facilitates the entrance of the bacterium and its dispersion to adjacent cells, leading to apoptosis and destruction of the intestinal epithelium. In particular, the bacterium induces local responses, localised in the invasion area (Tran Van Nhieu *et al.*, 2013), as well as global responses, that spread in the whole invaded cell. The local versus global character of the responses plays a crucial role in the cytotoxicity of the bacteria, since a high and sustained Ca^{2+} elevation can lead to cellular death and could limit the dissemination of the bacteria. Preliminary work regarding the atypical calcium responses caused by *Shigella* was carried out by Tran Van Nhieu *et al.* (2013) and Sun, *et al* (2017), using experimental methods and mathematical modelling. Nevertheless, the models that have been proposed do not take into account the Ca^{2+} coming from the extracellular space, which has been demonstrated to have a crucial contribution to the Ca^{2+} responses.

In this work we present a reactive-diffusive mathematical model that takes into account extracellular Ca^{2+} entry through ion channels located in the cell membrane (ROCC, SOCC), Ca^{2+} exchanges with the endoplasmic reticulum, as well as Ca^{2+} and IP_3 diffusion through the cytosol. The proposed model is capable to reproduce the calcium oscillations in the cytosol and in the endoplasmic reticulum observed in healthy cells, as well as the atypical calcium responses caused by *Shigella*. The model also allow us to analyse the global or local character of the

cytosolic calcium responses during bacterial invasion. Simulations using the proposed model showed that the rate of IP_3 synthesis is a bifurcation parameter that changes the stability of the system and that the entrance to the oscillatory regime has a dependence on the operation of ROCC and SOCC. Furthermore, spatio-temporal simulations showed that plasma membrane channels are clearly related to the global/local character of the calcium responses, which suggest that extracellular calcium entry through plasma membrane channels, particularly SOCC, could be a point of control of the bacterial invasion.

Resumen

UAM-A
División de Ciencias Básicas e Ingeniería

Master Degree in Process Engineering

Simulación de la dinámica espacio-temporal de Ca^{2+} durante la invasión de *Shigella*

Por

Roberto Ornelas Guevara

La shigelosis es un problema preocupante de salud pública a nivel mundial. Ésta es adquirida principalmente mediante la ingestión de comida o agua contaminadas con la bacteria *Shigella*. Después de ser ingerida, la bacteria invade el colon y causa una intensa reacción inflamatoria que concluye en la destrucción del tejido epitelial. Durante la etapa de invasión de las células epiteliales del intestino, la *Shigella* induce señales de Ca^{2+} atípicas; sin embargo, no es claro cómo se generan estas señales ni se sabe cómo controlarlas (Tran Van Nhieu *et al.*, 2013). Es bien sabido que las células utilizan Ca^{2+} intracelular como segundo mensajero en una gran cantidad de funciones celulares, incluyendo, por ejemplo, la reorganización del citoesqueleto, las respuestas inflamatorias y la muerte celular programada (apoptosis). Se ha informado en la literatura que la pertubación de las señales de Ca^{2+} intracelular causada por la *Shigella* facilita su entrada a las células y su dispersión a células adyacentes, lo que lleva a la apoptosis y destrucción del epitelio intestinal. En particular, la bacteria induce respuestas de Ca^{2+} locales en la célula invadida, localizadas en el sitio de invasión, así como respuestas globales, las cuales se difunden en toda la célula invadida. El carácter local y global de las respuestas celulares juega un papel crucial en la citotoxicidad y velocidad de invasión de la bacteria, debido a que una elevación alta y sostenida de Ca^{2+} intracelular ocasiona muerte celular temprana. Tran Van Nhieu *et al.* (2013) y Sun *et al.* (2017) llevaron a cabo trabajos preliminares de las respuestas de Ca^{2+} atípicas inducidas por la *Shigella*, utilizando métodos experimentales y modelado matemático. Sin embargo, los modelos reportados no toman en cuenta el Ca^{2+} proveniente del medio extracelular, el cual se ha demostrado que tiene una contribución clave en las respuestas locales y globales de Ca^{2+} de la célula invadida.

En este trabajo presentamos un modelo matemático reactivo-difusivo que toma en cuenta la entrada de Ca^{2+} extracelular al citosol a través de canales iónicos localizados en la membrana celular (ROCC y SOCC), intercambio de Ca^{2+} con el retículo endoplásmico y difusión de Ca^{2+} e IP_3 en el citosol. El modelo propuesto no solo reproduce las oscilaciones de Ca^{2+} citosólico y del retículo endoplásmico observadas en células sanas, sino que también es capaz de simular las condiciones causadas por la bacteria *Shigella*. El modelo propuesto también permite analizar el índice global o local de las respuestas de Ca^{2+} producidas por la invasión bacteriana. Las simulaciones obtenidas mediante nuestro modelo muestran que la velocidad de síntesis de IP_3 es

un parámetro de bifurcación que cambia la estabilidad del sistema y que la entrada y salida del régimen oscilatorio depende del funcionamiento de los canales ROCC y SOCC. Más aún, las simulaciones espacio-temporales permitieron verificar que estos canales se relacionan claramente con el índice global/local de las respuestas de Ca^{2+}, lo que sugiere que la entrada de Ca^{2+}extracelular a través de estos canales puede ser un punto de control de la invasión bacteriana.

Contents viii

List of figures

Chapter 1

Introduction

Shigellosis is an important problem of public health worldwide. It is mainly caused by the ingestion of food or water contaminated with *Shigella*. After ingestion, the bacterium invades the colon and causes an intense inflammatory reaction, leading to the destruction of the epithelial tissue.

The virulence of *Shigella* depends on a type III secretion system (T3SS), a needle-like structure, by which the bacterium injects virulence factors that causes, among other things, reorganisation of the actin cytoskeleton and regulation of inflammatory responses (Puhar *et al.*, 2013). Those events allow the bacterium to enter the host cell to replicate in it, and to disperse to adjacent cells. During cell invasion, *Shigella* induces atypical local and global calcium signals, but their role in invasion has remained unclear (Tran Van Nhieu *et al.*, 2013).

Almost every cell type uses Ca^{2+} as a second messenger to control a wide array of cellular functions, including reorganisation of the cytoskeleton, inflammatory responses and paths of cellular death (Sun *et al.*, 2017). Cells have evolved mechanisms by which they can tightly regulate their cytoplasmic [Ca^{2+}], both in space and time, via specific Ca^{2+} transporters. Those are localised in the plasma membrane, but also in the membrane of organelles such as endoplasmic reticulum, mitochondria or lysosomes.

The perturbation of cellular Ca^{2+} homeostasis caused by *Shigella*, not only facilitates the entrance of the bacterium and its dispersion to adjacent cells, but it also leads to apoptosis

and destruction of the intestinal epithelium (Bonnet and Tran Van Nhieu, 2015); Thus, the bacterium tightly controls the spatio-temporal aspects of Ca^{2+} dynamics to use efficiently the Ca^{2+} signals for its invasion, without inducing the death of its host too quickly.

Thus, it is necessary to disentangle and understand the link between the spatio-temporal dynamics of intracellular Ca^{2+} and bacterial invasion.

Therefore, the main goal of this project is to applicate tools provided by process engineering in order to construct a mathematical model that can describe the relationship between the dynamics of Ca^{2+} responses and *Shigella* invasion. In particular, we carried out simulations to analyse the importance of plasma membrane channels in the Ca^{2+} responses caused by *Shigella*.

1.1 State of the art

Shigella invasion in epithelial cells depends on a group of proteins called Ipa (IpaA, IpaB, IpaC and IpgD) (Invasion Plasmid Antigen), which are synthesised by the bacteria only after having contact with the host cell. The proteins are injected into the cytosol via the T3SS, notably to reorganise the actin cytoskeleton and to modulate inflammatory responses (Carayol and Tran Van Nhieu, 2013). The effector IpgD has been recently identified, and it has been demonstrated that it has a fundamental role in bacterial invasion (Niebuhr *et al.*, 2002; Konradt *et al.*, 2011; Mellouk *et al.*, 2014; Boal *et al.*, 2016; Weiner *et al.*, 2016). The influence of *Shigella* effectors in different stages of bacterial invasion has been widely studied (Tran Van Nhieu and Sansonetti, 1999; Bourdet-Sicard *et al*, 2000; Tran Van Nhieu *et al*, 2003; Parsot, 2009).

Nevertheless, few researchers have addressed the role of Ca^{2+} as a second messenger in the hijacking of cellular processes by pathogens, despite its importance (Sun, 2017). Tran Van Nhieu *et al.* (2013) showed that during cell invasion, *Shigella* induces transient peaks in cytosolic Ca^{2+} that depends on the T3SS, by which the bacterium injects IpaB and IpaC. Those triggers signals that result in actin polymerization, favouring the entrance of other bacterial effectors into the cytosol, further reorganising the actin cytoskeleton and modifying the synthesis and diffusion of inositol 1,4,5-trisphosphate (IP_3) through the cytosol.

Furthermore, Tran Van Nhieu *et al.* (2013) have shown that IP_3-mediated Ca^{2+} signalling is necessary for *Shigella* invasion. The bacterium triggers the recruitment of IP_3 receptors and phospholipases C (PLC-β y PLC-δ1) at invasion sites, and causes the accumulation of IP_3 at invasion sites through a diffusion-hindrance process. This phenomenom is fundamental to produce sustained raises in local Ca^{2+} responses during invasion. In order to identify the relationship between the dynamics of cytosolic IP_3 and Ca^{2+} during bacterial invasion, the authors used a mathematical model proposed by Dupont and Swillens (1996); although this approach is interesting, it rejects the dynamics of Ca^{2+} in the endoplasmic reticulum, and, therefore, does not allow to study the influence of an important Ca^{2+} entry mechanism known as SOCC (Store-Operated Calcium Channels), which may play an important role in the locality of Ca^{2+} responses and could suppose a point of control of the bacterial invasion. The so-called SOCC has been demonstrated to contribute to the frequency of Ca^{2+} oscillations, and thus may impact critical cellular functions; for example, it has been shown that in epithelial cells lacking of STIM1,

ORAI1 or TRPC1, there are deficiencies in Ca^{2+} influx and, therefore, in Ca^{2+} responses that are necessary for the correct function of the epithelium (Hong *et al.*, 2011). In Croisier *et al*. (2013) the authors proposed a mathematical model which describes the intracellular Ca^{2+} dynamics in airway smooth-muscle cells (ASMC) including SOCC, proving that it could be fundamental in the frequency of oscillations induced by agonists.

More recent evidence regarding *Shigella* invasion (Sun *et al.*, 2017) shows the importance of the bacterial effector IpgD in *Shigella* invasion, that hydrolyzes phosphatidylinositol-(4,5)bisphosphate and thus dampens IP_3 levels . By modifying IP_3 dynamics and diffusion, bacterial effector IpgD favors the elicitation of long-lasting local Ca^{2+} signals at *Shigella* invasion sites and converts *Shigella*-induced global oscillatory responses into erratic responses with atypical dynamics and amplitude. IpgD thus acts as a pathogen regulator of the Ca^{2+} code implicated in a versatility of cell functions. The authors used the model developed in Tran Van Nhieu *et al*. (2013) and carried out stochastic simulations for a more realistic approximation. Fig. 1 shows the modification in intracellular IP_3 dynamics in presence of IpgD.

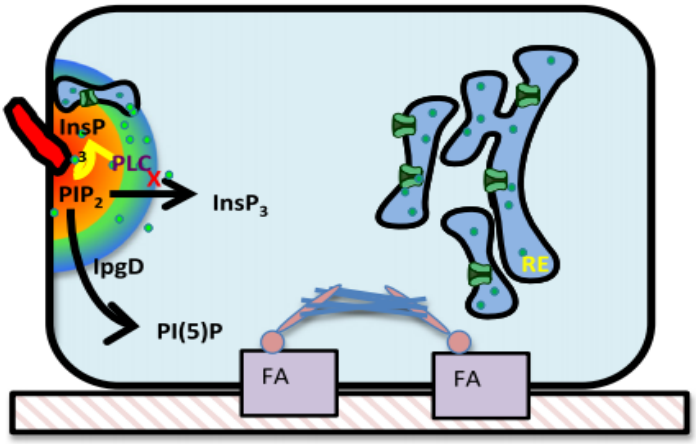

***Figure 1.1**:* IpgD hydrolyzes PI(4,5)P_2 thereby limiting the substrate pool available to PLCs at bacterial invasion sites. This results in a decrease in IP_3 production which, combined with restricted diffusion, favors long-lasting local Ca^{2+} at Shigella-induced actin foci (Sun *et al*., 2017).

1.2 The calcium signalling toolkit

Free [Ca^{2+}] in the cytosol ([Ca^{2+}]$_{cyt}$) has complex spatio-temporal properties. In the spatial domain, cells can activate highly localised [Ca^{2+}] responses -termed local responses- or, in some circumstances, can cause whole-cell responses -termed global responses-; In the temporal domain, specific information can be efficiently encoded in the frequency of calcium signals through an intrincate concert of action between several Ca^{2+} transporters. Frequency modulated Ca^{2+} oscillations represent a highly diverse signalling system that can regulate numerous processes in many different cell types. The cell is equipped with frequency decoding molecules that can translate oscillatory Ca^{2+} signals and activate specific cellular programs (Smedler and Uhlén, 2013).

The regulation of the different Ca^{2+} profiles are mediated by calcium channels, calcium pumps and receptors located in the plasma membrane and in internal stores. In the following, we will describe each component and their roles in Ca^{2+} dynamics.

1.2.1 IP_3, receptors and agonists

In practically every eukaryotic cell, changes in $[Ca^{2+}]_{cyt}$ are initiated by the binding of an agonist to a G-Protein Coupled Receptor (GPCR), forming a complex that transmits signals from the outside to the inside of the cell (Dupont *et al*., 2017). GPCR triggers the phosphatidylinositol signalling pathway, by which a G_q protein activates phospholipase C (PLC), an enzyme that is crucial to produce diacylglycerol (DAG) and IP_3 from phosphatidylinositol 4,5-bisphosphate (PIP_2). IP_3 can diffuse through the cytosol until it binds to IP_3 receptors (IPR). IPR is a Ca^{2+} channel localised in the membrane of the endoplasmic reticulum (ER). The binding of IP_3 opens this receptor, inducing Ca^{2+} release from the ER to the cytosol due to the concentration gradients between these two compartments. Ca^{2+} ions also binds to IPRs, increasing their open probability at low cytosolic $[Ca^{2+}]$, and thus causing release of Ca^{2+} from the ER in an auto-catalytic process known as Calcium Induced Calcium Release (CICR) (Dupont and Sneyd, 2017). IPRs are closed by high $[Ca^{2+}]$ in the cytosol.

1.2.2 Calcium influx

The rate of entry of Ca^{2+} into the cell is an important modulator of intracellular Ca^{2+} dynamic in all cell types (Dupont *et al*., 2017). In epithelial cells, the principal Ca^{2+} entry pathways are Store-Operated Calcium Channels (SOCC), the underlying molecular

mechanisms of which have been recently discovered (Smyth *et al*., 2010; Soboloff *et al*., 2012), and Receptor-Operated Calcium Channels (ROCC).

Activation of SOCC (see figure 1.2) occurs when the [Ca^{2+}] in the ER is low (Putney, 1986). Generally, depletion of Ca^{2+} in the ER is caused by IP_3-induced release. The major components of the SOCC pathway are the Stromal Interaction Molecules (STIM), embedded in the ER, which are sensitive to Ca^{2+} in the ER. The dissociation of Ca^{2+} from their ER binding site induces a conformational change in STIM, resulting in the formation of oligomers that translocate to the ER/plasmic membrane contact sites, where STIM proteins bind to Orai and/or TRP, the proteins forming the pore of SOCC, and trigger their opening (Croisier *et al*., 2013).

At first it was believed that the main function of SOCC was to prevent the depletion of intracellular Ca^{2+} deposits; however, recent studies suggest that the Ca^{2+} that enters through this mechanism is directly related to the activation of signalling events (Hong, *et al.*, 2011*;* Avila-Medina *et al.*, 2018; Pan, 2012*).*

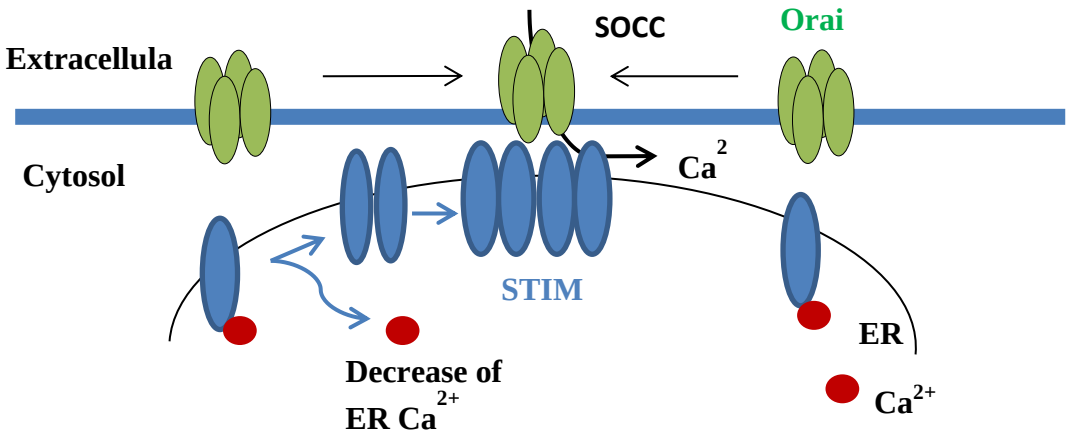

Figure 1.2*:* Molecular mechanism of SOCC activation. (Dupont and Sneyd (2017))

The molecular identity of the ROCC pathway isn't very clear. The principal difference between ROCC and SOCC is that while the latter depends on the [Ca^{2+}] within the ER, ROCC is independent of the ER but involves one or several of the signalling molecules resulting from the stimulation of PLC activity, IP_3 being the most relevant.

1.2.3 Calcium removal from the cytoplasm

Sarcoplasmic/Endoplasmic Reticulum Calcium ATPases (SERCA) and Plasma Membrane Calcium ATPases (PMCA) play a major role in the maintenance of low Ca^{2+} levels in the cytosol. PMCA pumps extrude Ca^{2+} to the extracellular space, whereas SERCA return Ca^{2+} to the internal stores. Both ATPases transport ions against their concentration gradient across a biological membrane by hydrolysis of ATP. They consume one molecule of ATP to pump two calcium ions.

1.2.4 Calcium oscillations

Oscillations of cytosolic [Ca^{2+}] are a well-known kind of signalling. The oscillations are often initiated by the binding of agonist (hormones, neurotransmitters, etc.) to GPCRs. The activation of GPCR is associated with the phosphatidylinositol signaling pathway, which is responsible to produce IP_3 and DAG. The IP_3 diffuses in the cytosol until it binds to IPRs that are located in the membrane of the ER, triggering Ca^{2+} release from the ER to the cytosol. In non-excitable cells, the repetitive calcium spikes mainly arise through the periodic exchange of Ca^{2+} between the ER and the cytosol, through the interplay between IPRs and SERCA pumps and Ca^{2+}. Indeed, this ion induces a fast and

explosive activation of IPRs, but also a slow inhibition of the receptors. The basic mechanism of Ca^{2+} can be seen in Figure 1.2.

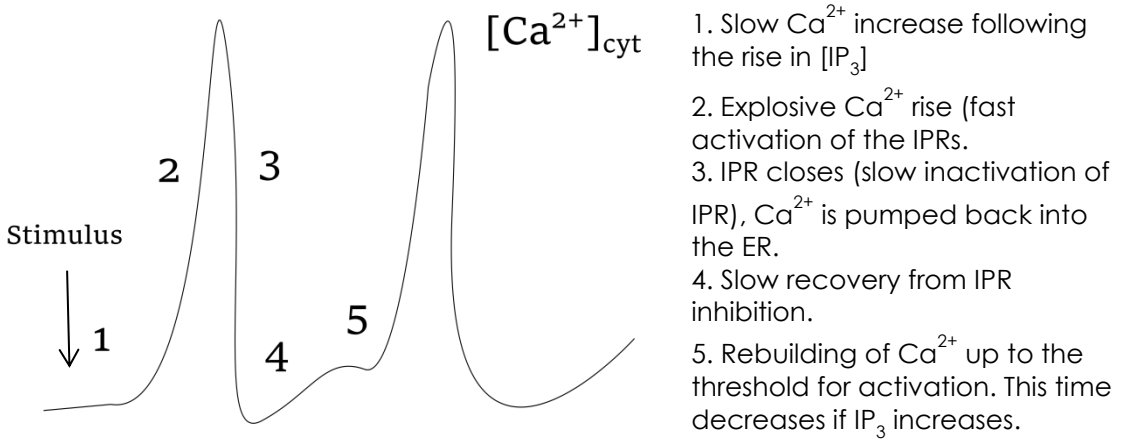

***Figure 1.3**:* Basic mechanism of cytosolic Ca^{2+} oscillations in non-excitable cells. These oscillations are initiated by the stimulus-induced rise in IP_3 concentration and ocurr trough a repetitive exchange of Ca^{2+} between the cytoplasm and the ER (Dupont and Combettes (2016))

Chapter 2

Project Approach

2.1 Hypothesis

Extracellular Ca^{2+} entry to the cytosol through SOCC is crucial to produce local and global Ca^{2+} responses induced by *Shigella* invasion in epithelial cells.

2.2 Justification

Shigellosis is considered as a major public health, causing an average of 167 million of diarrhea episodes and over a million deaths worldwide (Jenkins, 2015).

Shigella, the bacterium that is responsible for the disease, causes changes in the spatio-temporal dynamics of intracellular Ca^{2+} that are crucial for its virulence. Nevertheless, this remains poorly studied despite its importance; a good option to support the understanding of this physiological phenomenon is applying mathematical modelling and simulation tools that can help us to study the relationship between Ca^{2+} signalling in epithelial cells and *Shigella* invasion.

2.3 Aims

2.3.1 General Aim

Simulate the spatio-temporal dynamics of intracellular Ca^{2+} induced by *Shigella* invasion in epithelial cells.

2.3.2 Particular Aims

1. Develop a mathematical model that includes extracellular Ca^{2+} entry to the cytosol through SOCC.
2. Evaluate the importance of Ca^{2+} diffusion during invasion.
3. Simulate local and global Ca^{2+} responses induced by *Shigella*.

2.4 Procedure

This work will focus on simulate and analyze the importance of including extracellular Ca^{2+} entry to the cytosol through SOCC during *Shigella* invasion in epithelial cells.

To reach the aims, the following activities will be carried out:

1. Proposal of a mathematical model to describe calcium oscillations including SOCC, considering a well-mixed cell model.
2. Solve the proposed model considering diffusion of Ca^{2+} and IP_3 in order to take into account the conditions caused by *Shigella*.
3. Analysis of local and global Ca^{2+} responses induced by *Shigella*.

Chapter 3

Mathematical modelling

3.2 Mathematical modelling

3.2.1 Well-mixed cell approach

The most basic way to model calcium signalling is assuming a spatially homogeneous cell. In this configuration, we consider that the same [Ca^{2+}] and [IP_3] are seen in every point of the cell.

Here we extend the model proposed by Dupont and Swillens (1996) by including Ca^{2+} entry from the extracellular space through ROCC and SOCC, in order to study the impact of extracellular calcium entry on the calcium oscillations.

The Ca^{2+}-regulating mechanisms that are considered in the modelling approach are schematized in figure 3.1. and are the following:

Ca^{2+} flux between the extracellular medium and the cytosol

- J_{PMCA} (Plasma membrane calcium ATPase)
- J_{ROCC} (Receptor-Operated Calcium Entry)
- J_{SOCC} (Store-Operated Calcium Entry)

Ca^{2+} flux between the RE and the cytosol

- J_{SERCA} (Sarco-Endoplasmic Reticulum Calcium ATPase)

- J_{rel} (IP_3 receptor)

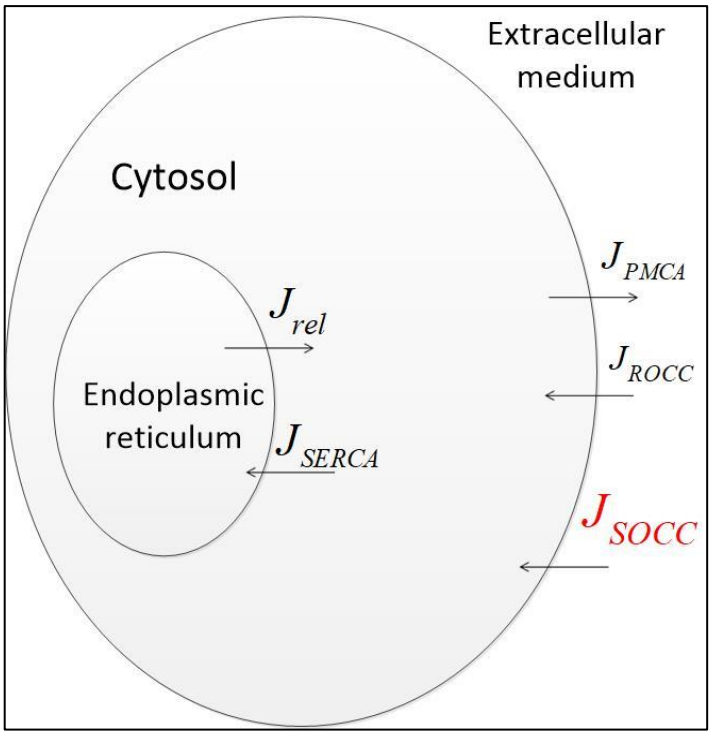

Figure 3.1*:* Scheme of Ca^{2+} fluxes in a spatially homogeneous cell (Dupont, 2017)

3.2.2 Ca^{2+} balance in the cell

To develop the Ca^{2+} oscillations model we assume that the concentration of Ca^{2+} and IP_3 are the same in any point of the cell (fig. 3.1). We denote C and c_s as the concentrations of Ca^{2+} in the cytosol and the ER, respectively.

Through the law of mass conservation we can say that

$$\left(Ca^{2+}\ \text{accumulation}\right) = \begin{pmatrix} Ca^{2+}\ \text{entering} \\ \text{the cytosol} \end{pmatrix} - \begin{pmatrix} Ca^{2+}\ \text{leaving} \\ \text{the cytosol} \end{pmatrix}$$

In mathematical notation, considering the volumes of the cytosol and ER as constants, the evolution equations for $[Ca^{2+}]$ are defined below:

$$\frac{dC}{dt} = J_{in} + J_{rel} - J_{PMCA} - J_{SERCA} \tag{3.1}$$

$$\frac{dc_s}{dt} = J_{SERCA} - J_{rel} \tag{3.2}$$

The fluxes are expressed by the following equations:

- Ca^{2+} entry into the cytosol

$$J_{in} = J_{SOCC} + J_{ROCC} + J_{leak} \tag{3.3}$$

- Ca^{2+} entry into the cytosol through SOCC (Croisier *et al.* (2013))

$$J_{SOCC} = V_s P_{so} \tag{3.4}$$

where V_s is the maximal Ca^{2+} flux through SOCC and P_{so} is a variable describing the fraction of STIM proteins linked to Orai proteins.

- Ca^{2+} entry into the cytosol through ROCC

$$J_{ROCC} = \alpha_1 I \tag{3.5}$$

where α_1 is a constant and I is a variable describing the evolution of $[IP_3]$

- Ca^{2+} leak from the extracellular medium

$$J_{leak} = \alpha_0 \tag{3.6}$$

where α_0 is a constant.

- Ca^{2+} fluxes through SERCA and PMCA pumps

$$J_{SERCA} = V_e \frac{C^2}{K_e^2 + C^2} \tag{3.7}$$

$$J_{PMCA} = V_p \frac{C^2}{K_p^2 + C^2} \tag{3.8}$$

where *Ve* and *Vp* are the maximum rate of Ca^{2+} pumping through SERCA and PMCA, respectively, whereas *Ke* and *Kp* denote the SERCA and PMCA affinities to Ca^{2+}, respectively.

- Ca^{2+} release from endoplasmic reticulum via IPRs

$$J_{rel} = k_1 \left(c_s - C \right) \left(b + R_a \right) \tag{3.9}$$

where k_1 is the IPR rate, *b* is a Ca^{2+} leak from the ER and R_a is the fraction of open IPRs.

- Fraction of STIM proteins linked to ORAI proteins (Croisier *et al.* (2013))

$$\frac{dP_{so}}{dt} = \left(\frac{K_s^4}{K_s^4 + c_s^4} - P_{so} \right) / \tau_s \tag{3.10}$$

where $\frac{K_s^4}{K_s^4 + c_s^4}$ can be interpreted as the fraction of STIM proteins dissociated from the ER as a consequence of its Ca^{2+} depletion, and thus able to oligomerise and move toward the PM to bind with Orai and/or TRP. *Ks* is the affinity for C_s and τ_s is the SOCC timescale.

- Intracellular IP_3 dynamics (Tran Van Nhieu *et al*, 2003)

$$\frac{dI}{dt} = V_b + J_{IP} - k_d I \tag{3.11}$$

where V_b is the basal synthesis of IP_3, J_{IP} is the IP_3 stimulated synthesis due to *Shigella* and k_d is the rate of IP_3 degradation.

- Fraction of activated IP_3R (Dupont and Swillens, 1996) (See Appendix E)

$$R_a = (1 - R_i)\frac{I}{K + I}\frac{C^{na}}{K_A^{na} + C^{na}} \tag{3.12}$$

where R_i is the fraction of inhibited IPRs, K is the affinity of the IPRs for IP_3, K_A is the affinity constant of the activating site of the IPR for Ca^{2+} and *na* is the Hill coefficient of Ca^{2+} binding to the activating site of the IPR

- Fraction of inhibited IPRs (Dupont and Swillens, 1996) (See Appendix E)

$$\frac{dR_i}{dt} = k_+\left(1 - R_i\right)\frac{C^{ni}}{1 + \left(\frac{C}{K_A}\right)^{na}} - k_- R_i \tag{3.13}$$

where k_+ is the rate constant of Ca^{2+} binding to the inhibiting site of the IPR, k_- is the rate of Ca^{2+} dissociation from the IPR inhibiting site, *ni* is the Hill coefficient of Ca^{2+} binding to the inhibiting site of the IPR and K_A the affinity constant of the activating site of the IPR for Ca^{2+}

Substituting the fluxes expressions in equations (3.1) and (3.2), and adding the parameters α and γ, which are, respectively, the volumic ratio between the ER and the cytosol and viceversa, the following mathematical model is obtained:

$$\frac{dC}{dt} = \alpha_0 + \alpha_1 I + V_s P_{so} + \alpha k_1\left(Ra + b\right)\left(c_s - C\right) - V_e\frac{C^2}{K_e^2 + C^2} - V_p\frac{C^2}{K_p^2 + C^2} \tag{3.14}$$

$$\frac{dI}{dt} = V_b + J_{IP} - k_d I \tag{3.15}$$

$$\frac{dc_s}{dt} = \gamma\left(V_e \frac{C^2}{K_e^2 + C^2}\right) - k_1\left(Ra + b\right)\left(c_s - C\right) \tag{3.16}$$

$$\frac{dR_i}{dt} = k_+\left(1 - R_i\right)\frac{C^{ni}}{1 + \left(\frac{C}{K_A}\right)^{na}} - k_- R_i \tag{3.17}$$

$$\frac{dP_{so}}{dt} = \left(\frac{K_s^4}{K_s^4 + c_s^4} - P_{so}\right) / \tau_s \tag{3.18}$$

Table 3.1. List of parameter values

Parameter	***Definition***	***Value***	***Source***
α_0	Constant Ca^{2+} influx leak	0	Croisier et al., (2013)
α_1	ROCC rate	$0.00105 s^{-1}$	Croisier et al., (2013)
V_s	Maximal rate of Ca^{2+} pumping through SOCC	$1.57 \mu M / s$	Croisier et al., (2013)
V_P	Maximal rate of Ca^{2+} pumping through PMCA	$0.1 \mu M / s$	O'Donnell & Owen, (1994)
K_P	PMCA affinity	$1 \mu M$	O'Donnell & Owen, (1994)
k_1	IPR rate	$0.4 s^{-1}$	This work
b	Ca^{2+} leak rate from ER	$7(10)^{-3} s^{-1}$	Tran Van Nhieu et al., (2013)
V_e	Maximal rate of Ca^{2+} pumping through SERCA	$1.1 \mu M / s$	Lytton, J. *et al*., (1992)
K_e	SERCA affinity	$0.275 \mu M$	Lytton, J. *et al*., (1992)
V_b	Basal rate of IP_3 synthesis	$0.1 - 1 \mu M / s$	This work
J_{IP}	Stimulated rate of IP_3 synthesis at the site of the bacterium	$0 \mu M / s$	
k_d	First order rate constant of IP_3 degradation	$0.1 s^{-1}$	Tran Van Nhieu et al., (2013)
γ	Volumic ratio between the cytosol and the ER	20	Tran Van Nhieu et al., (2013)
k_-	Rate constant of Ca^{2+} dissociation from this site	$0.005 s^{-1}$	Tran Van Nhieu et al., (2013)
k_+	Rate constant of Ca^{2+} binding to the inhibiting site of the IPR	$0.1822 \mu M^{-3} s^{-1}$	Tran Van Nhieu et al., (2013)

Continue

ni	Hill coefficient of Ca^{2+} binding to the inhibiting site of IPR	3	Tran Van Nhieu et al., (2013)
na	Hill coefficient of Ca^{2+} binding to the activating site of IPR	2	Tran Van Nhieu et al., (2013)
K_s	STIM ER Ca^{2+} affinity	$200\mu M$	Luik *et al.*, (2008)
τ_s	SOCC timescale	$30s$	Croisier et al., (2013)
K_A	Affinity constant of the activating site of the IPR for Ca^{2+}	$0.4\mu M$	Tran Van Nhieu et al., (2013)
K	Affinity of the IPR for IP_3	$1\mu M$	Tran Van Nhieu et al., (2013)
α	Volumic ratio between the ER and the cytosol	0.05	Tran Van Nhieu et al., (2013)

3.2.3 Validation

In order to validate the model described by equations 3.14-3.18, we choose the affinity constants of PMCA and SERCA pumps, as well as their maximum flux rates of Ca^{2+}, all within physiological ranges (O'Donnell and Owen, 1994; Lytton, J. *et al*., 1992) so that in the simulations we can observe:

1. Ca^{2+} oscillations in physiological levels (Dupont *et al.,* 2017)
2. Contraphase between [Ca^{2+}] in the cytosol and in the ER (Ishii *et al.,* 2006).
3. Decrease in the period of oscillations with respect to a greater presence of IP_3 in the cytosol.
4. Lower [Ca^{2+}] in the ER as IP_3 synthesis increases (Mikoshiba and Hattori (2000)), (5) greater activation of the fraction of STIM proteins linked to ORAI proteins as the synthesis of IP_3 increases and (6) increase in the period of Ca^{2+} oscillations in the absence of Ca^{2+} flux from the extracellular medium to the cytosol (Ishii *et al,* 2006)

Figure 3.2A shows sustained Ca^{2+} oscillations triggered by 1μM [IP_3], followed by an increase in Ca^{2+} period caused by a decrease in IP_3 concentration. In the same figure, one

can observe that the ER [Ca^{2+}] is in counterphase with cytosolic Ca^{2+} and gets higher while IP_3 is decreasing. Our model thus reproduces successfully the points 1-4.

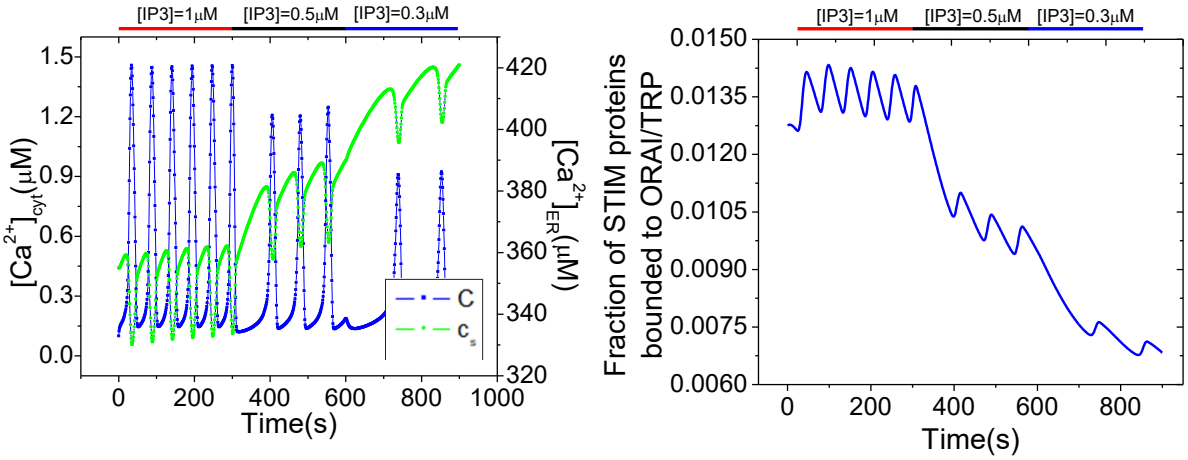

Figure 3.2: Simulation using Eqs. 3.14-3.18 and the parameter values in table 1 for (A) Dynamics of Ca^{2+} exchanges between cytosol and ER. Different IP_3 concentrations (1μM, 0.5μM, 0.3μM) are obtained by considering different V_b values (0.1μM, 0.05μM and 0.03μM, respectively), (B) evolution of the fraction of STIM proteins bounded to Orai/TRP proteins.

Another important fact that the model must predict is the increase in the Ca^{2+} flux thorugh SOCC associated to growing [IP_3]. In figure 3.2B it is possible to appreciate that the fraction of STIM proteins linked to ORAI proteins will increase proportionally with the synthesis of IP_3. This is explained by a higher [IP_3] leading to a greater Ca^{2+} release from the IP_3 receptors, which causes the ER to reach lower Ca^{2+} levels. These low levels trigger a greater dissociation of STIM proteins that that travel through the plasma membrane until they reach the Orai/TRP proteins, thus being able to activate in a greater proportion SOCC and allowing a greater influx of Ca^{2+} thorugh it.

This fact makes clear the importance of the participation of SOCC in the modeling of Ca^{2+} oscillations during bacterial invasion, since, as mentioned, the bacterial effectors cause accumulation, and therefore, an increase of IP_3 in sites of invasion, causing a

greater flux of Ca^{2+} from the RE to the cytosol, which leads to a greater depletion of it, causing a more relevant participation of SOCC.

The modification in the period of oscillations without the presence of extracellular Ca^{2+} has been studied by Ishii, et al (2006). They used fluorescent green protein (GFP) indicators to measure [Ca^{2+}] in the cytosol and the ER, and found a decrease of approximately 30% in the period of cytosolic Ca^{2+} oscillations if they do not add Ca^{2+} in the extracellular medium. In figure 3.3 it can be seen that the model is able to reproduce this effect in the period of Ca^{2+} oscillations in the absence of extracellular calcium

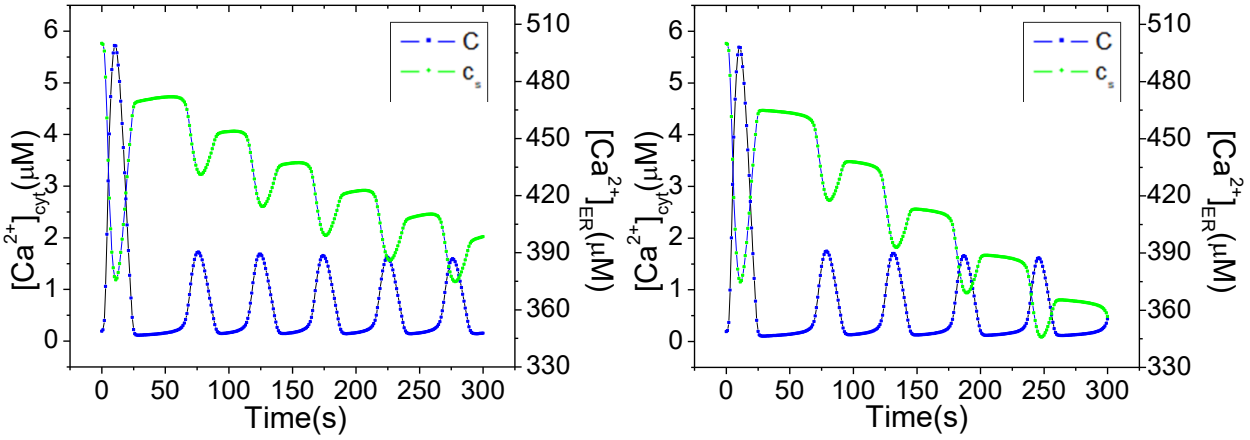

Figure 3.3*:* Simulation using Eqs. 3.14-3.18 and the parameter values in table 1 and Vb=0.1μM for Ca^{2+} oscillations in the cytosol and in the ER with (A) and without (B) Ca^{2+} entry from the extracellular medium.

3.3 Spatio-temporal cytosolic Ca^{2+} responses during *Shigella* invasion

Tran Van Nhieu *et al.*, (2013) have shown that during *Shigella* invasion, the bacterium induces atypical long-lasting local Ca^{2+} responses, termed RATPs for Responses

Associated With Trespassing Pathogens, that depend on the confinement of IP_3 and enrichment of IP_3 receptors (IPRs) at bacterial entry sites. These confined Ca^{2+} signals occurring within the vicinity of the plasma membrane could directly regulate Ca^{2+} dependent processes, including cortical actin reorganization, which is necessary for bacterial invasion. Later, Sun *et al.* (2017) found that the diffusive characteristics and the rate of IP_3 synthesis are both important in defining the local versus global character of the Ca^{2+} response, which is crucial for the cytotoxicity of the bacteria. The main limitation for studying the local vs. global responses induced by the bacterium with the model used in Tran Van Nhieu *et al.* (2013) and Sun *et al.* (2017) is that it does not consider the Ca^{2+} entry into the cytosol from the extracellular space nor the dynamics of Ca^{2+} in the ER (which is necessary since it activates SOCC). Consequently, this model does not allow the analysis of Ca^{2+} responses considering different conditions of Ca^{2+} entry from the extracellular space.

The model developed in chapter 3.1 take the mechanisms of Ca^{2+} entry into account, but it is not suited to study the local vs. global character since it is a well-mixed cell model. In order to make the model suitable for studying the influence of external Ca^{2+} in the global/local Ca^{2+} responses caused by *Shigella*, it is necessary to consider the spatial heterogeneity in the cell. To model and understand such spatially distributed behavior, inclusion of Ca^{2+} and IP_3 diffusion is necessary, so in the following, Fickian diffusion will be briefly described.

3.3.1 Fickian diffusion

The diffusive process can be defined as the transfer of molecules through a fluid by means of individual and disordered displacements. The net movement of molecules is always from a region of high chemical potential to a region of low chemical potential. A proper way to describe this process is with the molar flux, described as vector quantity denoting the amount of the particular species, in molar units, that passes per given increment of time through a unit area normal to the vector. The flux may be defined with reference to coordinates that are fixed in space (Welty *et al.*, 1984).

The basic relation for diffusion defines the molar flux relative to the molar-average velocity (J_A) is the Fick's first law, which defines the diffusion of component A in a system B in steady state:

$$J_A = -D_{AB}\nabla C_A \tag{3.19}$$

For diffusion in the x direction, the Fick rate equation is

$$J_{A,x} = -D_{AB}\left(\frac{dC_A}{dx}\right) \tag{3.20}$$

To take the time curse of the diffusion into account, it is necessary to make a mass balance over a volume, which is

$$\begin{pmatrix}\text{accumulation of}\\ \text{component A}\\ \text{in the volume } \Delta x\Delta y\Delta z\end{pmatrix} = \begin{pmatrix}\text{rate of}\\ \text{mass of A in}\end{pmatrix} - \begin{pmatrix}\text{rate of}\\ \text{mass of A out}\end{pmatrix}$$

Mathematically, it is expressed by

$$\left(\Delta x \Delta y \Delta z\right)\frac{dC_A}{dt} = \left(\Delta y \Delta z\right)\left(J_A\Big|_x - J_A\Big|_{x+\Delta x} \right) \tag{3.21}$$

Dividing eq. (3.21) by $\left(\Delta x \Delta y \Delta z\right)$ and taking the limit as $\Delta x \to 0$

$$\frac{\partial C_A}{\partial t} = -\frac{\left(\partial J_A\right)}{\partial x} \tag{3.22}$$

Substituting Fick's first law in eq. (3.22) we get,

$$\frac{\partial C_A}{\partial t} = D_{AB}\frac{\partial^2 C_A}{\partial x^2} \tag{3.23}$$

Eq. (3.23) is known as Fick's second law, for directions x and y it takes the form,

$$\frac{\partial C_A}{\partial t} = D_{AB}\left(\frac{\partial^2 C_A}{\partial x^2} + \frac{\partial^2 C_A}{\partial y^2}\right) = D_{AB}\nabla^2 C_A \tag{3.24}$$

3.3.2 Global Ca^{2+} responses and adding diffusion to the well-mixed cell model

In some cell types, Ca^{2+} oscillations occur practically uniformly across the cell. In such situation, measurement of the [Ca^{2+}] at any point of the cell gives the same time course, and a well-mixed model is appropriate. However, intracellular waves of Ca^{2+} often accompany Ca^{2+}oscillations (Berridge, 1993); in most cases, the [Ca^{2+}] first increases locally, and this local rise then propagates in the whole cell as a wave (Dupont *et al.*, 2017).

To consider spatially distributed Ca^{2+} dynamics in the model developed in chapter 3, one can simply add Fickian diffusion expressions to the differential equations describing $[Ca^{2+}]$ and $[IP_3]$ in the whole-cell model (Dupont *et al*, 2017), which gives,

$$\frac{\partial C}{\partial t}=\alpha_0+\delta\left(\alpha_1 I+V_s P_{so}\right)+\alpha k_1\left(Ra+b\right)\left(c_s-C\right)-V_e\frac{C^2}{K_e^2+C^2}-V_p\frac{C^2}{K_p^2+C^2}+D_c\nabla^2 C \tag{3.25}$$

$$\frac{\partial I}{\partial t}=V_b+J_{IP}-k_d I+D_I\nabla^2 I \tag{3.26}$$

$$\frac{\partial c_s}{\partial t}=\gamma\left(V_e\frac{C^2}{K_e^2+C^2}\right)-k_1\left(Ra+b\right)\left(c_s-C\right)+Dc_s\nabla^2 c_s \tag{3.27}$$

$$\frac{dR_i}{dt}=k_+\left(1-R_i\right)\frac{C^{ni}}{1+\left(\frac{C}{K_A}\right)^{na}}-k_- R_i \tag{3.28}$$

$$\frac{dP_{so}}{dt}=\left(\frac{K_s^4}{K_s^4+c_s^4}-P_{so}\right)/\tau_s \tag{3.29}$$

For the simulations, the diffusive terms were discretized using central finite differences (see section 3.3.4 and Appendix C) to get a semi-discretized model, which is a set of Ordinary Differential Equations (ODEs) that have to be integrated in every point of the mesh. The initial conditions in the simulations are those in which the system is at steady state for each case. To analyse the importance of ROCC and SOCC in the local/global responses of the system, the following cases are analysed: simulations with (i) normal Ca^{2+} flux conditions between the plasma membrane (PM) and the extracellular space; (ii)

blocking ROCC; (iii) blocking SOCC; partially blocking (iv) ROCC, (v) SOCC and (vi) partially blocking all extracellular calcium fluxes. The boundary conditions considered are no-flux conditions. A MATLAB code was made to carry out the simulations.

Regarding Ca^{2+} diffusion in the ER, it is not known exactly how Ca^{2+} diffuses in the lumen of the ER and its diffusion coefficient has not been definitely measured. Furthermore, the extremely intricate geometry of the ER makes its modelling too complicated, so in many cases it is sufficient to assume that the $[Ca^{2+}]$ in both the cytosol and the ER coexist at every point in space. Dayel *et al.* (1999) found diffusion within the ER lumen to be approximately 3-6 times slower than in the cytosolic bulk and they estimated the diffusion coefficient of Ca^{2+} in the ER lumen to be 5-10$\mu m^2/s$. In our model we use a diffusion coefficient equal to 10$\mu m^2/s$ to describe Ca^{2+} diffusion in the ER.

The geometry of the system is schematized in Figure 3.4.

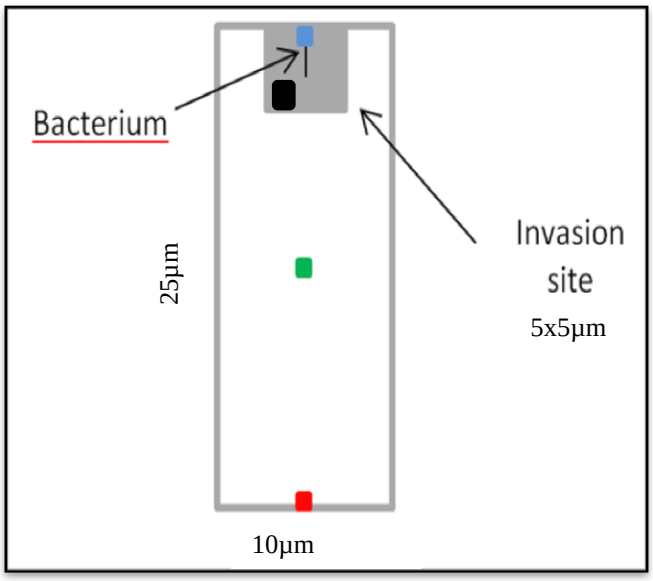

Figure 3.4: Geometry used in the simulations. At the invasion site (grey square), the diffusion coefficient of IP_3 and Ca^{2+} in the cytosol are 1.6 times smaller than in the remaining of the cytosol and the density of IP_3 receptors is 1.5 times higher. Stimulated IP_3 synthesis occurs at the locus of the black rod representing the bacterium (Van Nhieu *et al.*, 2013).

3.3.3 Setting the conditions caused by *Shigella*

To include the conditions caused by the bacterium, non-homogeneities in the next parameters must be considered (Tran Van Nhieu *et al.*, (2013)):

1. The rate of stimulated IP_3 synthesis, J_{IP}. This term is restricted to a portion of the invasion site (black bar in Fig. 3.4) that is supposed to represent the bacterium. Its value is equal to 0.79μM and 0.7μM, for $D_I = 280\mu m^2 / s$ and $D_I = 10\mu m^2 / s$, respectively, which causes a response similar to that observed in experimental data (Tran Van Nhieu *et al*, 2013)

2. The diffusion coefficients of IP_3 (D_I) and Ca^{2+} (D_C) in the invasion area. Both parameters are 1.6 smaller in this area than in the rest of the cell.

3. The maximal rate of Ca^{2+} release through the IP_3 receptor (k_1). As this parameter represents the product of the channel conductance by the density of receptors, changes in k_1 values correspond to changes in receptors density in the invasion area. Its value is 1.5 times higher in the invasion area than in the rest of the cell (Sun *et al*, 2017)

The diffusion coefficients for cytosolic Ca^{2+} and IP_3 were taken from Tran Van Nhieu *et al* (2013). Nevertheless, recent work by Dickinson *et al.* (2017) suggest that the value of the diffusion coefficient for IP_3 in the cytosol is about 30 fold slower than previously reported, so in this work will be carried out some simulations using a IP_3 coefficient diffusion equal to $10\mu m^2/s$.

3.3.4 Numerical scheme

To simulate the model including spatial effects, a two dimensional rectangular mesh (64x20) is considered. The system is described as an array of coupled systems of ODEs. The basic system is described by equations 3.14-3.18, which has the next form,

$$\frac{dC\left(C,I,R_i\right)}{dt} = f_1\left(C,I,R_i\right) \tag{3.30}$$

$$\frac{dI\left(I\right)}{dt} = f_2(I) \tag{3.31}$$

$$\frac{dc_s\left(C,I,R_i,c_s\right)}{dt} = f_3\left(C,I,R_i,c_s\right) \tag{3.32}$$

$$\frac{dR_i\left(C,R_i\right)}{dt} = f_4(C,R_i) \tag{3.33}$$

$$\frac{dP_{so}\left(P_{so},c_s\right)}{dt} = f_5\left(P_{so},c_s\right) \tag{3.34}$$

With the following functions

$$f_1\left(C,I,R_i\right) = \alpha_0 + \alpha_1 I + V_s P_{so} + \alpha k_1\left(Ra+b\right)\left(c_s - C\right) - V_e\frac{C^2}{K_e^2+C^2} - V_p\frac{C^2}{K_p^2+C^2} \tag{3.35}$$

$$f_2(I) = V_b + J_{IP} - k_d I \tag{3.36}$$

$$f_3\left(C,I,R_i,c_s\right) = \gamma\left(V_e\frac{C^2}{K_e^2+C^2}\right) - k_1\left(Ra+b\right)\left(c_s - C\right) \tag{3.37}$$

$$f_4(C,R_i)=k_+\left(1-R_i\right)\frac{C^{ni}}{1+\left(\frac{C}{K_A}\right)^{\overline{na}}}-k_-R_i \tag{3.38}$$

$$f_5\left(P_{so},c_s\right)=\left(\frac{K_s^4}{K_s^4+c_s^4}-P_{so}\right)/\tau_s \tag{3.39}$$

The coupling is carried out adding three diffusive functions to the terms describing the $[Ca^{2+}]$ and $[IP_3]$ in the cytosol. Then, the system with n_x nodes in direction x and n_y nodes in direction y takes the form,

$$\frac{dC_{i,j}}{dt}=f_1\left(C_{i,j},I_{i,j},R_{i(i,j)}\right)+\Psi_{\mathrm{C}}(C_{i,j}) \tag{3.40}$$

$$\frac{dI_{i,j}}{dt}=f_2(I_{i,j})+\Psi_{\mathrm{I}}\left(I_{i,j}\right) \tag{3.41}$$

$$\frac{dc_{s(i,j)}}{dt}=f_3\left(C_{i,j},I_{i,j},R_{i(i,j)},c_{s_{(i,j)}}\right)+\Psi_{c_s}(c_{s_{(i,j)}}) \tag{3.42}$$

$$\frac{dR_{i(i,j)}}{dt}=f_4(C_{i,j},R_{i(i,j)}) \tag{3.43}$$

$$\frac{dP_{so(i,j)}}{dt}=f_5\left(P_{so_{(i,j)}},c_{s_{(i,j)}}\right) \tag{3.44}$$

With the following diffusive functions (see Appendix C for details of the finite differences formulation),

$$\Psi_{\mathrm{C}}(C_{i,j})=M_C(C_{i-1,j}+C_{i+1,j}-4C_{i,j}+C_{i,j+1}+C_{i,j-1}) \tag{3.45}$$

$$\Psi_{\mathrm{I}}(I_{i,j})=M_I(I_{i-1,j}+I_{i+1,j}-4I_{i,j}+I_{i,j+1}+I_{i,j-1}) \tag{3.46}$$

$$\Psi_{c_s}(c_{s_{(i,j)}}) = M_{c_s}(c_{s_{(i-1,j)}} + c_{s_{(i+1,j)}} - 4c_{s_{(i,j)}} + c_{s_{(i,j+1)}} + c_{s_{(i,j-1)}}) \quad (3.47)$$

Where $M_C = \frac{D_C}{(\Delta x)^2}$, $M_I = \frac{D_I}{(\Delta x)^2}$ and $M_{c_s} = \frac{D_{c_s}}{(\Delta x)^2}$

With $2 \le i \le n_x$ and $2 \le j \le n_y$ for equations 3.40-3.44.

The boundary conditions are no-flux conditions for both cytosolic IP_3 and Ca^{2+} in all the simulations.

Definitions and values of the parameters are given in Table 3.1, except for k_1, which, for this case, has a value equal to 0.1μM in order to reproduce the behavior showed in Tran Van Nhieu *et al* (2013) for the case without restrictive diffusion of IP_3 and Ca^{2+} in the invasion site. We use the commercial software MATLAB to solve the system of coupled ODEs using the function ode23. In figure 3.5 can be seen a flowchart of the algorithm used to simulate the Ca^{2+} responses caused by *Shigella*.

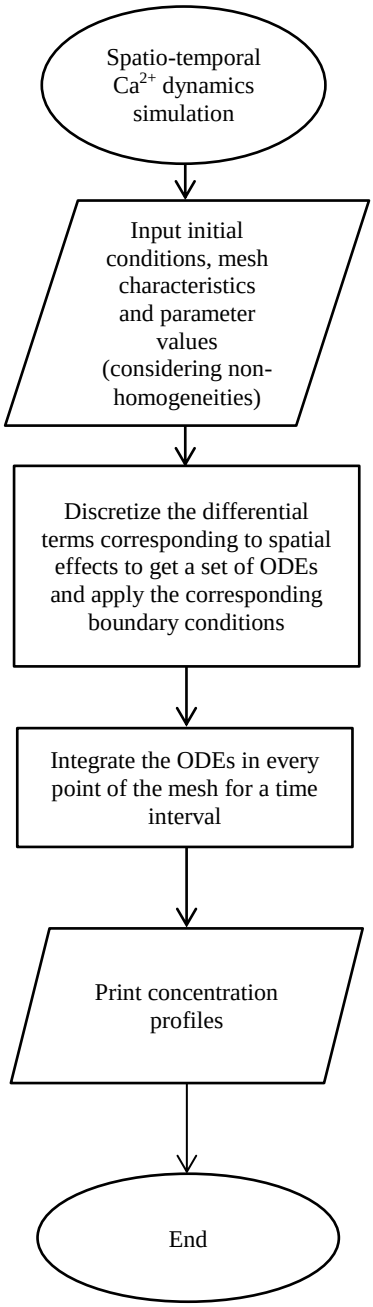

Figure 3.5: Flowchart of the method of lines to solve the model considering *Shigella* invasion.

Chapter 4

Results and discussions

4.1 Analysis of calcium entry through plasma membrane channels

The nature and regulation of the Ca^{2+} influx mechanisms are of special interest because the plasma membrane channels have shown promise as pharmacological targets (Putney & Bird, 2008), so in the following we will discuss the effect that ROCC and SOCC have on Ca^{2+} oscillations.

To analyse the importance of Ca^{2+} entry through the plasma membrane, three different cases were considered: (i) totally blocking SOCC; (ii) totally blocking ROCC and (iii) partially blocking SOCC and ROCC. For this last case, dimensionless parameter δ was introduced in Eq. (3.14) in order to control the relative magnitudes of Ca^{2+} entering the cell through plasma membrane channels.

The model is analysed considering the basal synthesis of IP_3 (V_b) as a bifurcation parameter. It is important to have an idea of how Ca^{2+} oscillations change for different values of IP_3 (via the parameter V_b), because its synthesis and its diffusion are modified during *Shigella* invasion (Tran Van Nhieu *et al.*, 2013).

In all the bifurcation diagrams, the green circles and the blue circles represent the minimum and the maximum of the stable and unstable limit cycles, respectively.

In fig. **4.1a** can be seen two Hopf bifurcations for $V_b = 0.0223\mu M$ and $V_b = 0.4412\mu M$, which are supercritical (HB_1) and subcritical (HB_2), as well as a limit point bifurcation (LP_1) at $V_b = 0.9498\mu M$. This implies that an oscillatory behavior is guaranteed only for the values of V_b that are between the two Hopf bifurcations. Between HB_2 and LP_1 oscillations may occur only for certain initial conditions. The red lines indicate the stable steady-states of the system whereas the black lines stand for the unstable ones. One can possible to notice that for very small and very high values of V_b the system presents stationary solutions. In fig. **4.1a** can be seen how the period of oscillations is reduced as the value of V_b increases, which is consistent with the fact that, for a higher synthesis of IP_3, the Ca^{2+} release of the IP_3 receptors is greater, causing a decrease in the period of oscillations. We observe from figure **4.1b** that considering a higher synthesis of IP_3, which is observed in invasion sites during *Shigella* invasion, the oscillatory regime goes to stationary.

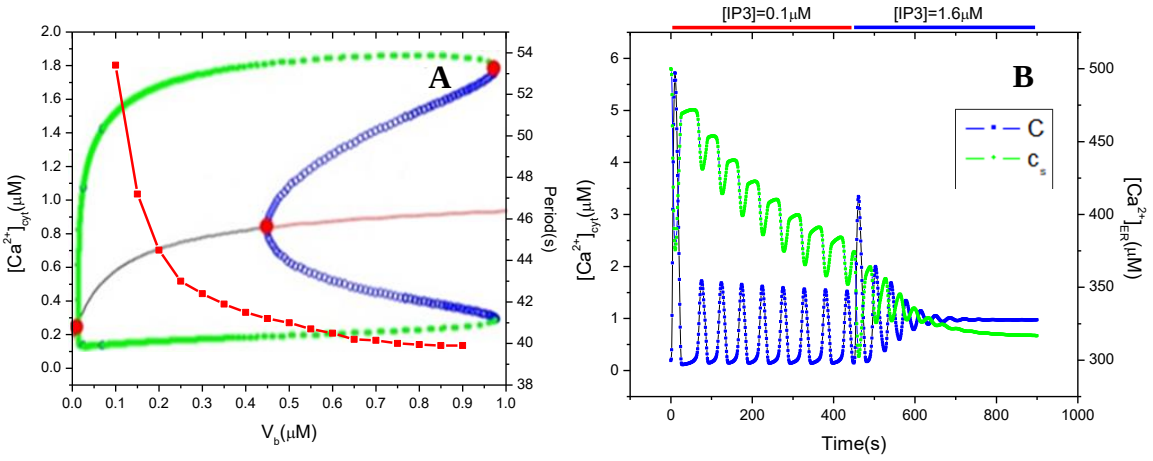

Figure 4.1: (A) Bifurcation diagram and period (red dotted line) of Ca^{2+} oscillations; (B) time series of the model described by equations (3.14-3.18), using parameters shown in table 3.1.

Figure 4.2 shows bifurcation and period diagrams, as well as time series partially blocking extracellular Ca^{2+} entry, with the aim of analyzing the impact of Ca^{2+} coming from them in the oscillatory responses of the system. In figure **4.2a**, the influx is reduced by a factor 2 ($\delta = 0.5$). One can see two Hopf bifurcations, one supercritical and one subcritical, and a LP bifurcation in $V_b = 0.02664\mu M$, $V_b = 1.42\mu M$ and $V_b = 3.47\mu M$, respectively. In figure **4.2c** the fluxes are reduced by a factor 10 ($\delta = 0.1$). The bifurcation diagram displays a pair of Hopf bifurcations, a pair of period doubling (PD) bifurcations and a LP bifurcation at $V_b = 0.0414\mu M$, $V_b = 28.81\mu M$, $V_b = 0.04236\mu M$, $V_b = 0.04272\mu M$ and $V_b = 34.16\mu M$, respectively. By observing these points, we can affirm that with a greater blocking of ROCC and SOCC, the oscillatory regime will be extended for higher values of IP_3 synthesis. In figures **4.2A** and **4.2C** it can be seen that the the period of oscillations increases significantly at low IP_3 values if ROCC and SOCC are blocked. In contrast with the effect caused by the increase in IP_3 synthesis shown in figure 4.1. This is improved by low values of δ (Fig. **4.2**)

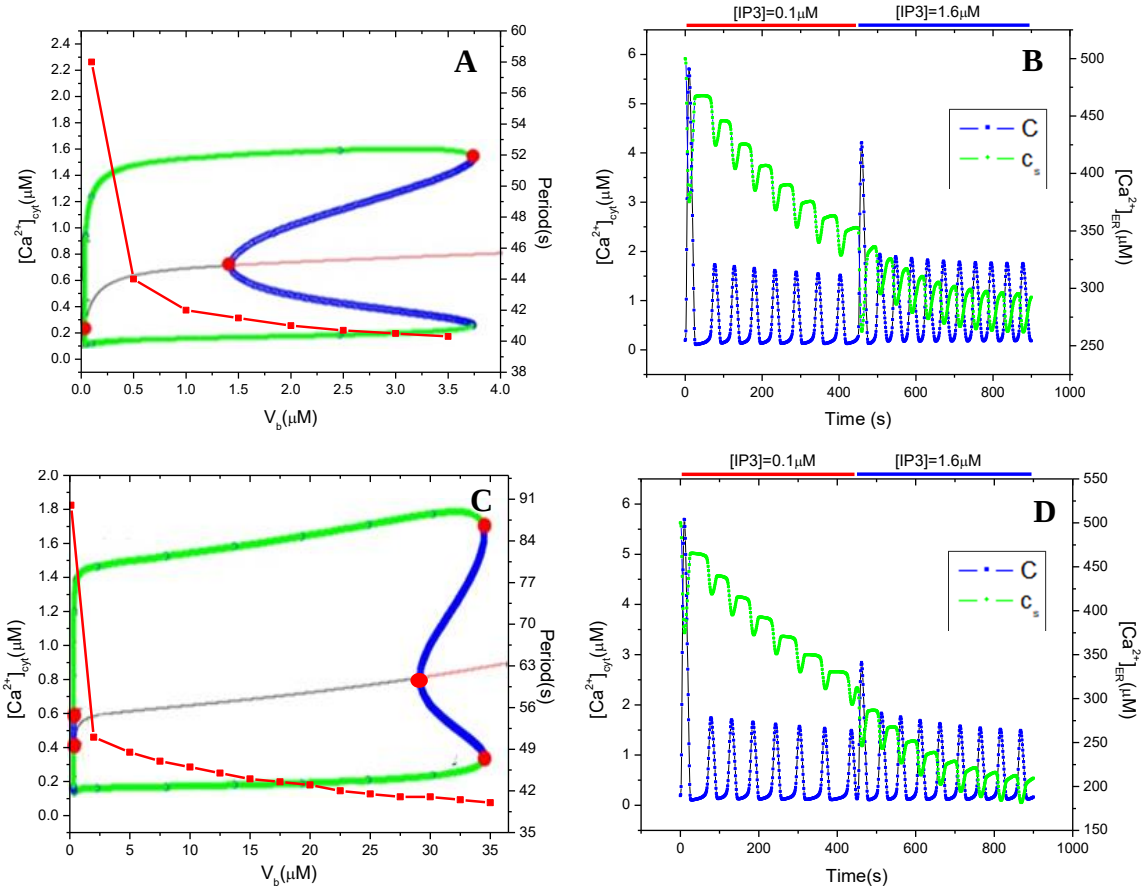

Figure 4.2: (A, C) Bifurcation diagrams and period (red dotted line) of Ca^{2+} oscillations; (B,D) time series of the model described by equations (3.14-3.18) using parameters shown in Table 3.1, Partially blocking extracellular Ca^{2+} for (A,B) $\delta = 0.5$ and (C,D) $\delta = 0.1$.

Figure **4.3** shows the impact of ROCC and SOCC separately on the stability of the system. By blocking ROCC (**4.3A**), it can be seen two Hopf bifurcations, supercritical and subcritical, and a LP bifurcation at $V_b = 0.02272\mu M$, $V_b = 0.5172\mu M$ and $V_b = 2.617\mu M$, respectively; blocking SOCC (**4.3C**) causes the appearance of two Hopf bifurcations (Supercritical and subcritical), a pair of PD bifurcations and a LP bifurcation at $V_b = 0.255\mu M$, $V_b = 3.686\mu M$, $V_b = 0.2634\mu M$, $V_b = 0.2692\mu M$ and $V_b = 3.89\mu M$, respectively. It is possible to notice that, blocking ROCC, the oscillatory regime between

the two HB does not vary much with respect to that observed in figure **4.1A**. However, depending on the initial conditions oscillatory regime could occur for larger values of basal synthesis of IP_3 with respect to Figure **4.1A**, due to the coexistence of a stable limit cycle and a stable steady-state between HB_2 and LP_1

For the case in which SOCC (**4.3C**) is completely blocked, it can be seen that the behavior of the system varies significantly with respect to that of fig. **4.1**. It is possible to see that oscillatory regime is presented for higher values of V_b; which suggests that, for some values of V_b that would cause steady state under normal conditions, blocking SOCC could induce a more robust Ca^{2+} oscillations.

In Figure **4.3A** can be seen that the period does not vary significantly with respect to that of physiological conditions; However, in figure **4.3C** can be seen that the period of oscillations increases significantly by completely blocking SOCC, suggesting that such a channel plays an important role in the shaping of the frequency of oscillations and, therefore, may impact critical cellular functions. It is interesting to see in figure **4.3B** that with closed ROCC the system still display oscillations with basal IP_3 synthesis (V_b=0.1μM) and with higher IP_3 synthesis (which is observed during *Shigellosis* in the invasion sites of the cell) (V_b=1.6μM), but blocking SOCC (figure **4.3C**) causes stationary regime with a basal IP_3 synthesis; nevertheless, considering higher IP_3 synthesis the stationary regime vanishes and the system presents oscillatory solutions.

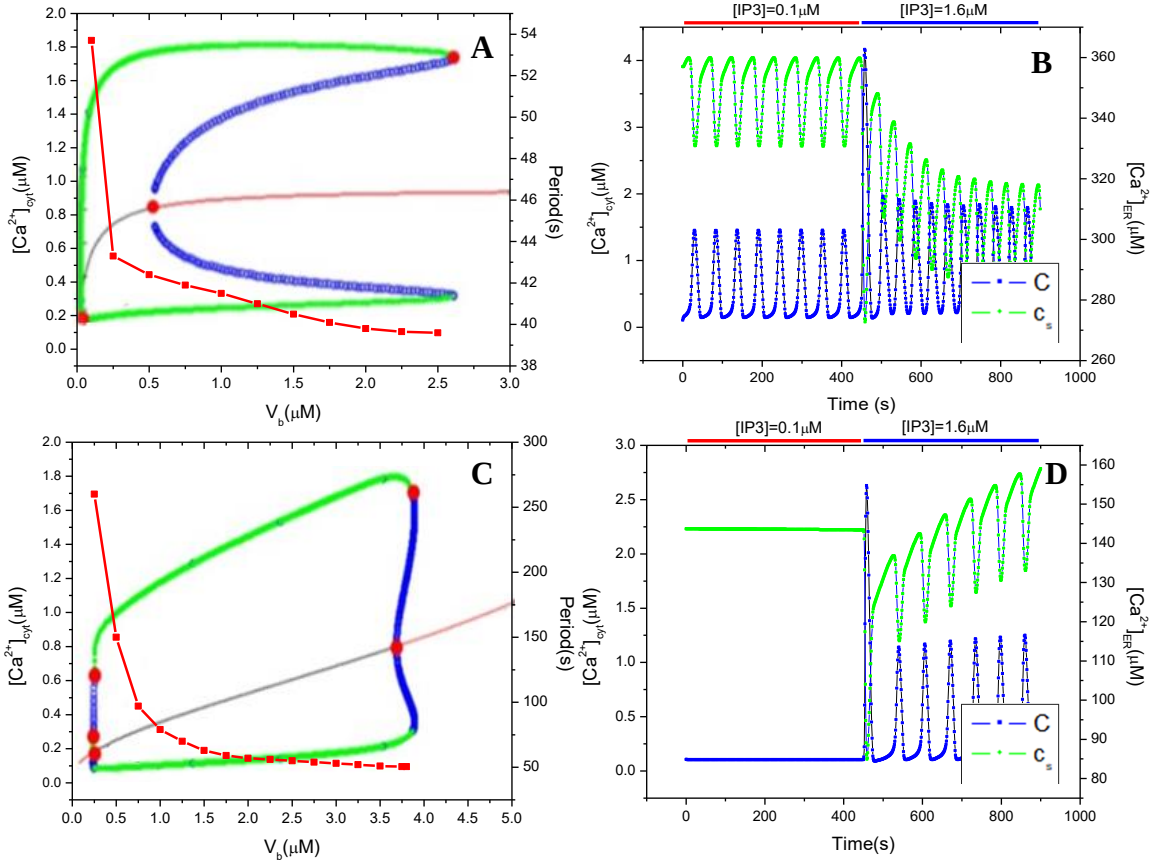

Figure 4.3: (A, C) Bifurcation diagrams and period (red dotted line) of Ca^{2+} oscillations; (B,D) time series of the model described by equations (3.14-3.18) using parameters shown in Table 3.1, Totally blocking J_{ROCC} (A,B) and J_{SOCC} (C,D).

4.2 Simulations of the spatio-temporal calcium responses during *Shigella* invasion

4.2.1 Dependence of RATPs on restricted diffusion

It has been demonstrated by Tran Van Nhieu *et al.* (2013) that *Shigella* stablish an actin meshwork that limits diffusion of free solutes, which is necessary to produce RATPs: without restricted diffusion of Ca^{2+} and IP_3 in invasion site, no significant local Ca^{2+} increase is observed. The model described by equations 3.25-3.29 is able to reproduce the responses without restricted diffusion, as can be seen in figure 4.5.

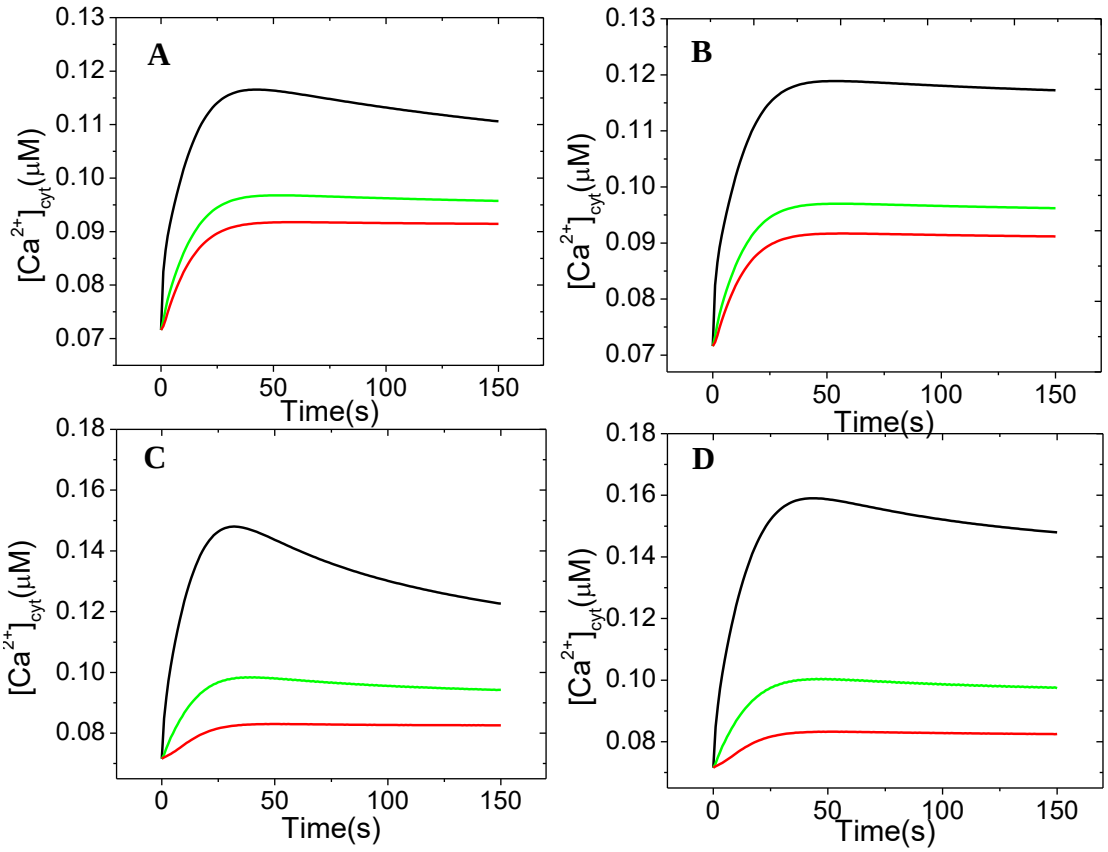

Figure 4.4: Evolution of $[Ca^{2+}]$ at the upper (invasion site)(black), medium (green) and lower point (red) using eqs. 3.25-3.29 considering Ca^{2+} and IP_3 diffusion in the cytosol, with all the conditions caused by the bacterium less restricted diffusion in the invasion area for the next cases: **(A)** $D_I = 280\mu m^2/s$ and without

diffusion of Ca^{2+} in the ER, **(B)** $D_I = 280\mu m^2/s$ and diffusion of Ca^{2+} in the ER, **(C)** $D_I = 10\mu m^2/s$ and without diffusion of Ca^{2+} in the ER, **(D)** $D_I = 10\mu m^2/s$ and diffusion of Ca^{2+} in the ER.

4.2.2 Effect of extracellular calcium on the responses caused by *Shigella*

As stated previously in this project, *Shigella* induces local and global intracellular Ca^{2+} responses in epithelial cells, which favour bacterial invasion and dissemination. The global versus local character of the responses plays a crucial role in the bacterial invasion, since the cytotoxicity of the bacterium depends of it.

Extracellular Ca^{2+} entry into the cytosol, particularly from the SOCC channels, have shown to be crucial to maintain and control calcium oscillations in different types of cells (Smyth *et al*., 2009), including epithelial cells (Hong *et al*., 2011). Consequently, we proposed to analyse the effect of these channels in the global/local character of the Ca^{2+} responses.

To analyse the influence of extracellular calcium on the global/local Ca^{2+} responses caused by *Shigella* in epithelial cells we considered the two values for the diffusion coefficient of IP_3 in the cytosol that we found in the literature (see section 3.3.4).

The following scenarios are considered: (i) $D_I = 280\mu m^2/s$ without Ca^{2+} diffusion in the ER; (ii) $D_I = 280\mu m^2/s$ with Ca^{2+} diffusion in the ER; (iii) $D_I = 10\mu m^2/s$ without Ca^{2+} diffusion in the ER, (iv) $D_I = 10\mu m^2/s$ with Ca^{2+} diffusion in the ER. With the aim to analyse the effect of SOCC and ROCC individually on the calcium responses caused by the bacterium, the parameters δ_{ROCC} and δ_{SOCC} were used to control the relative

magnitudes of the calcium fluxes coming from the plasma membrane channels, as can be seen in figure 4.4.

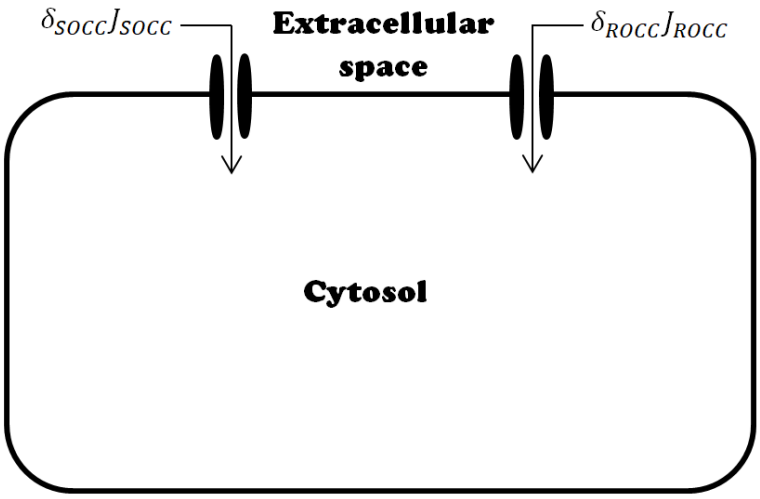

Figure 4.5: Schematic diagram of the control of the relative calcium fluxes through SOCC and ROCC, controlled by the parameters δ_{ROCC} and δ_{SOCC}.

In order to analise the local vs. global character of the Ca^{2+} responses caused by *Shigella* we define a Globality Coefficient (GC) as the ratio between the maximum value of the $[Ca^{2+}]$ in the invasion site (black square in figure 3.4) and in the cytosolic (red square in figure 3.4). The larger the GC, the more local the response.

The results of the simulations of spatio-temporal Ca^{2+} calcium dynamics for the four scenarios can be seen in figures **4.6-4.13.**

4.2.2.1 Scenario I: Fast IP_3 diffusion, without diffusion of Ca^{2+} in the ER

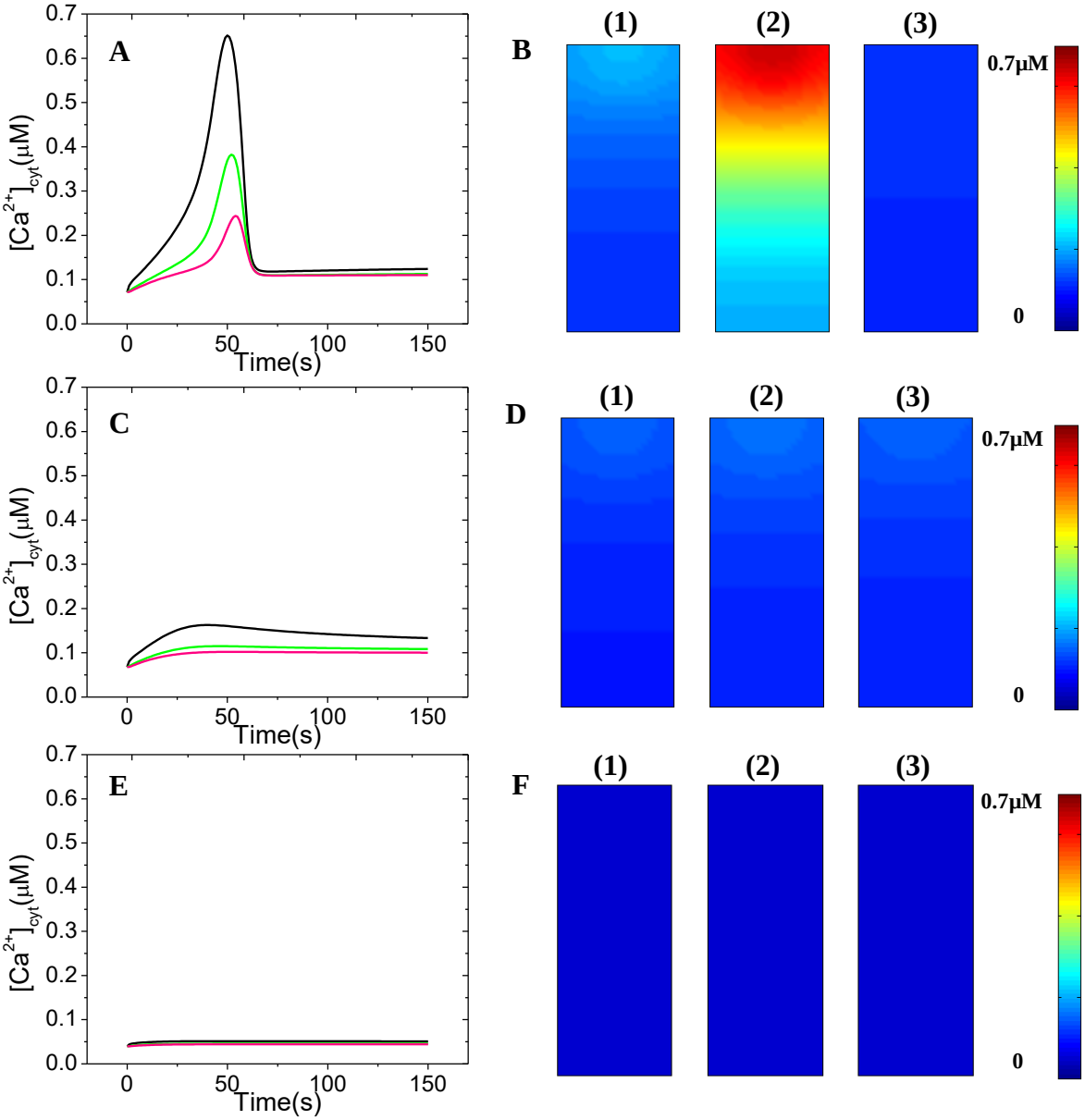

Figure 4.6: (Graphs in the left)Evolution of [Ca^{2+}] at the upper (invasion site)(black), medium (green) and lower point (red) in eqs 3.25-3.29 and the parameter values in table 1, except for V_b and k_1, whose values are, respectively, 0.01µM/s and $0.1s^{-1}$, considering Ca^{2+} and IP_3 diffusion in the cytosol, with all the conditions caused by the bacterium in the invasion site for the next cases: **(A)** normal extracellular Ca^{2+} entry conditions **(C)** Blocking ROCC; **(E)** Blocking SOCC. (Coloured maps in the right and relation to the graphs) Simulated levels of cytosolic Ca^{2+} at 25 (1), 50 (2) and 75s (3) after onset of bacterial invasion depicted in color scale with dark blue and red corresponding to 0 and 0.7µM, respectively, for **(B)** normal extracellular Ca^{2+} entry conditions; **(D)** blocking ROCC; **(F)** blocking SOCC. For $D_I = 280\mu m^2/s$, without diffusion of Ca^{2+} in the ER

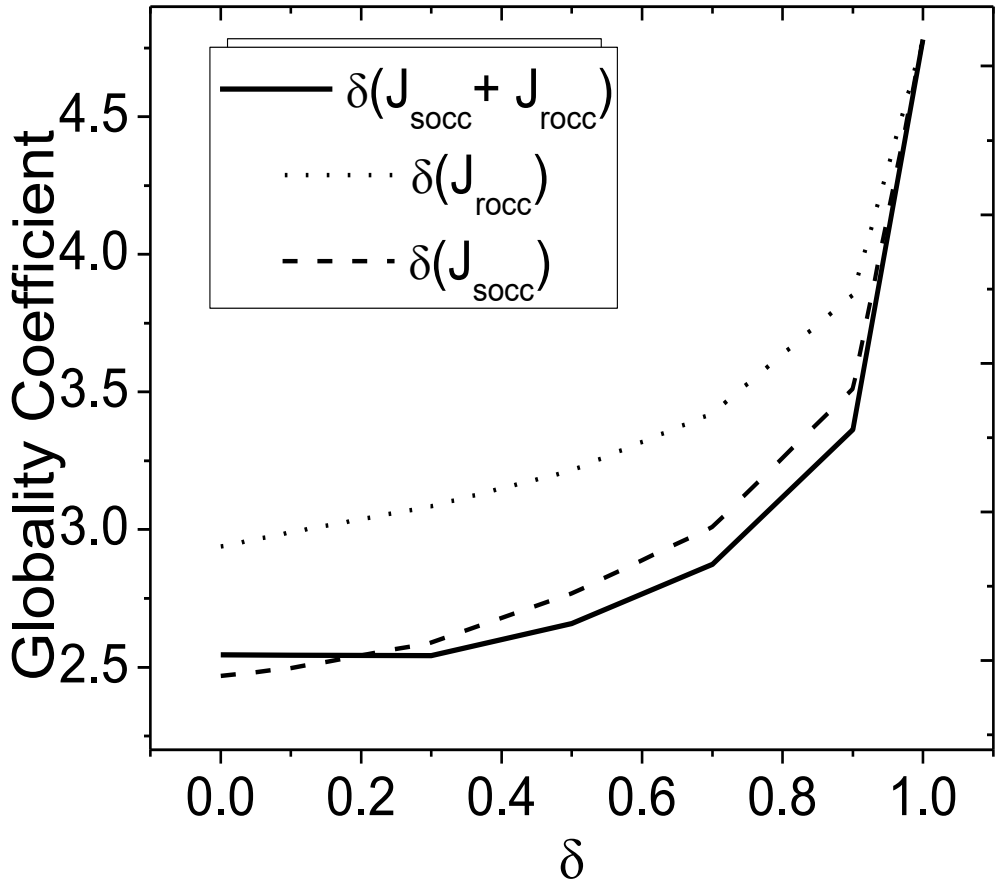

Figure 4.7: Globality coefficient considering $D_I = 280\mu m^2/s$ and without diffusion of Ca^{2+}in the ER

As can be seen in fig. **4.6**, SOCC seems to have a more crucial role in the calcium responses than ROCC, since completely blocking it, only a little elevation of $[Ca^{2+}]$ in the whole cell is seen. This case also predicts that completely blocking ROCC avoids RATPs to occur. In fig. **F.1** (see Appendix F), can be seen that, the more are blocked SOCC and ROCC (separately or both), the more the calcium responses diminish gradually until no response is seen.

4.2.2.2 Scenario II: Fast IP_3 diffusion, with diffusion of Ca^{2+} in the ER

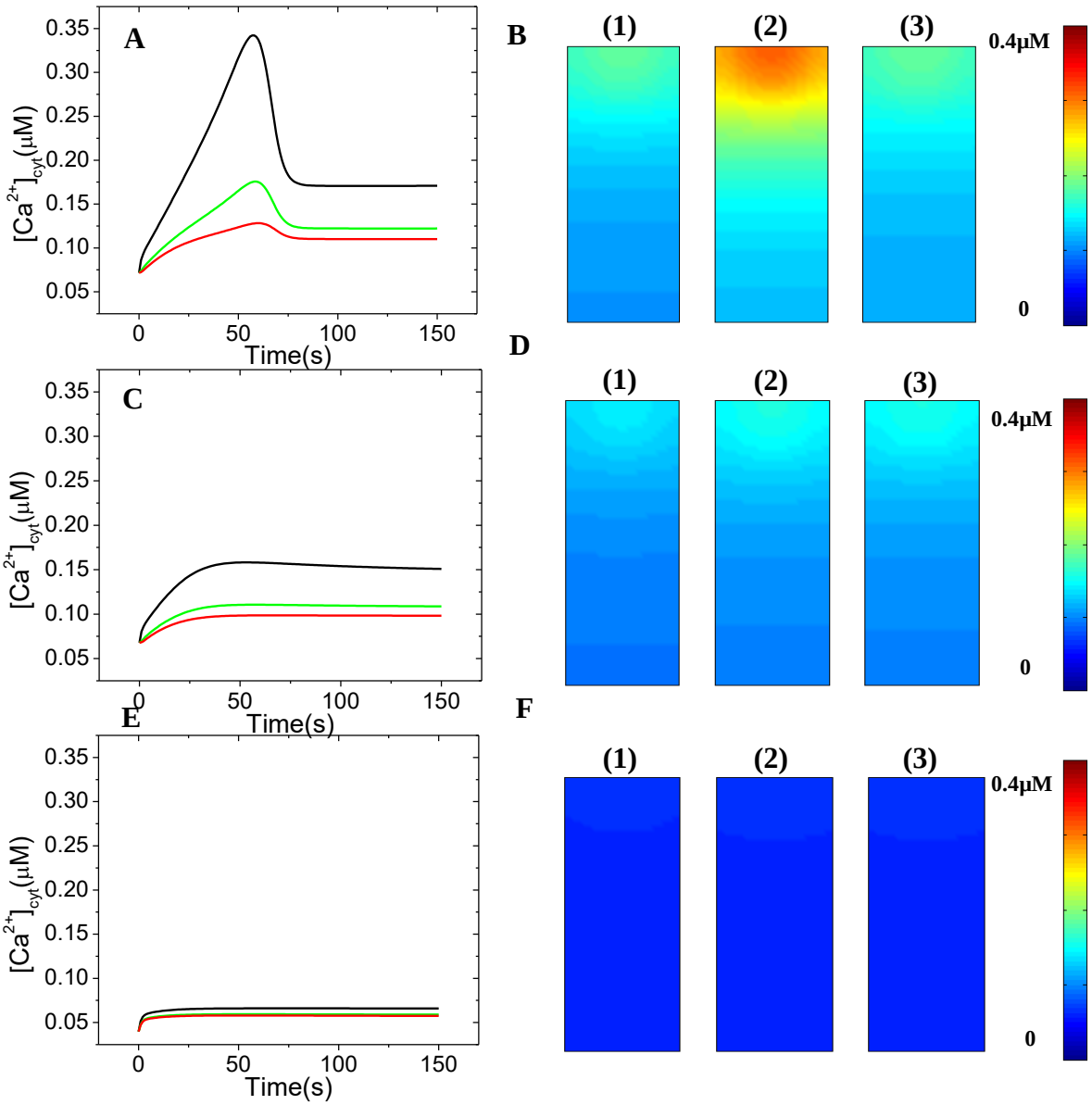

Figure 4.8: (Graphs in the left)Evolution of $[Ca^{2+}]$ at the upper (invasion site)(black), medium (green) and lower point (red) in eqs 3.25-3.29 and the parameter values in table 1, except for V_b and k_1, whose values are, respectively, 0.01μM/s and $0.1s^{-1}$, considering Ca^{2+} and IP_3 diffusion in the cytosol, with all the conditions caused by the bacterium in the invasion site for the next cases: **(A)** normal extracellular Ca^{2+} entry conditions **(C)** Blocking ROCC; **(E)** Blocking SOCC. (Coloured maps in the right and relation to the graphs) Simulated levels of cytosolic Ca^{2+} at 25 (1), 50 (2) and 75s (3) after onset of bacterial invasion depicted in color scale with dark blue and red corresponding to 0 and 0.4μM, respectively, for **(B)** normal extracellular Ca^{2+} entry conditions; **(D)** blocking ROCC; **(F)** blocking SOCC. For $D_I = 280\mu m^2/s$, considering diffusion of Ca^{2+} in the ER.

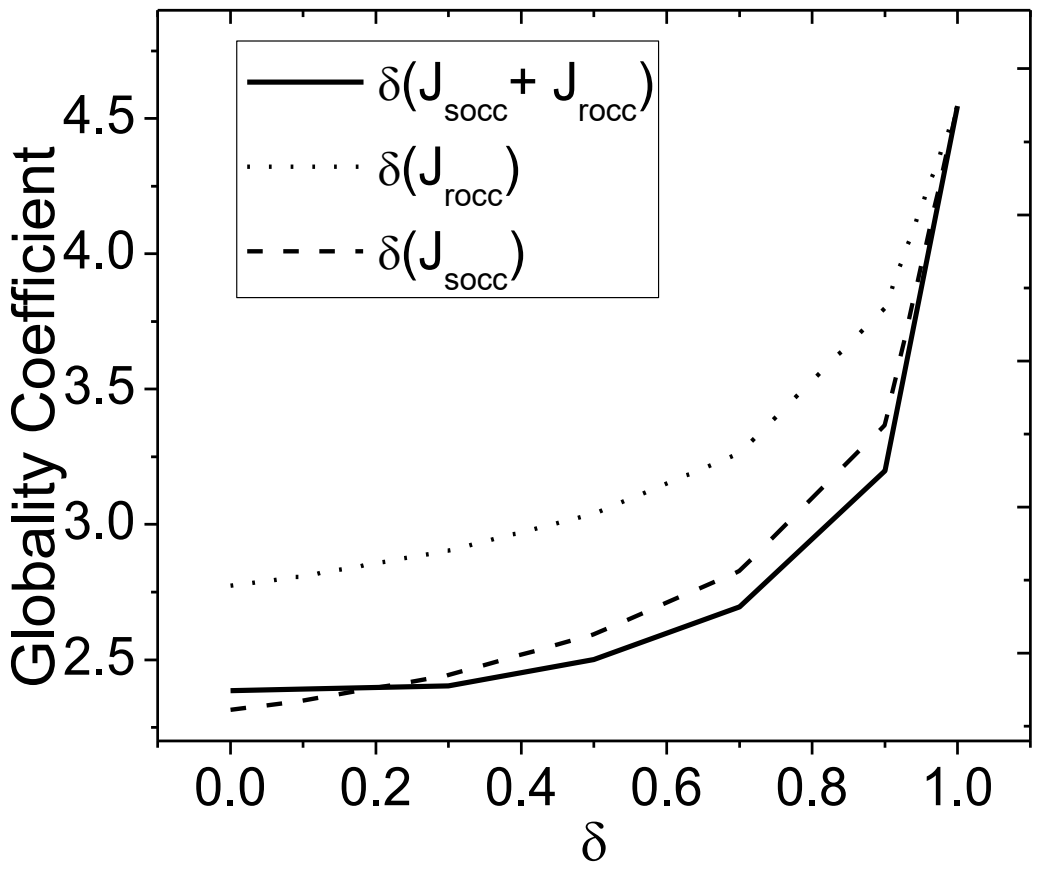

Figure 4.9: Globality coefficient considering $D_I = 280\mu m^2/s$ and with diffusion of Ca^{2+}in the ER

The results for scenario II are generally the same as scenario I, with the exception that in this case can be seen that the calcium response is lower, the amplitude of the response is larger and a higher basal concentration is reached.

4.2.2.3 Scenario III: Slow IP_3 diffusion, without diffusion of Ca^{2+} in the ER

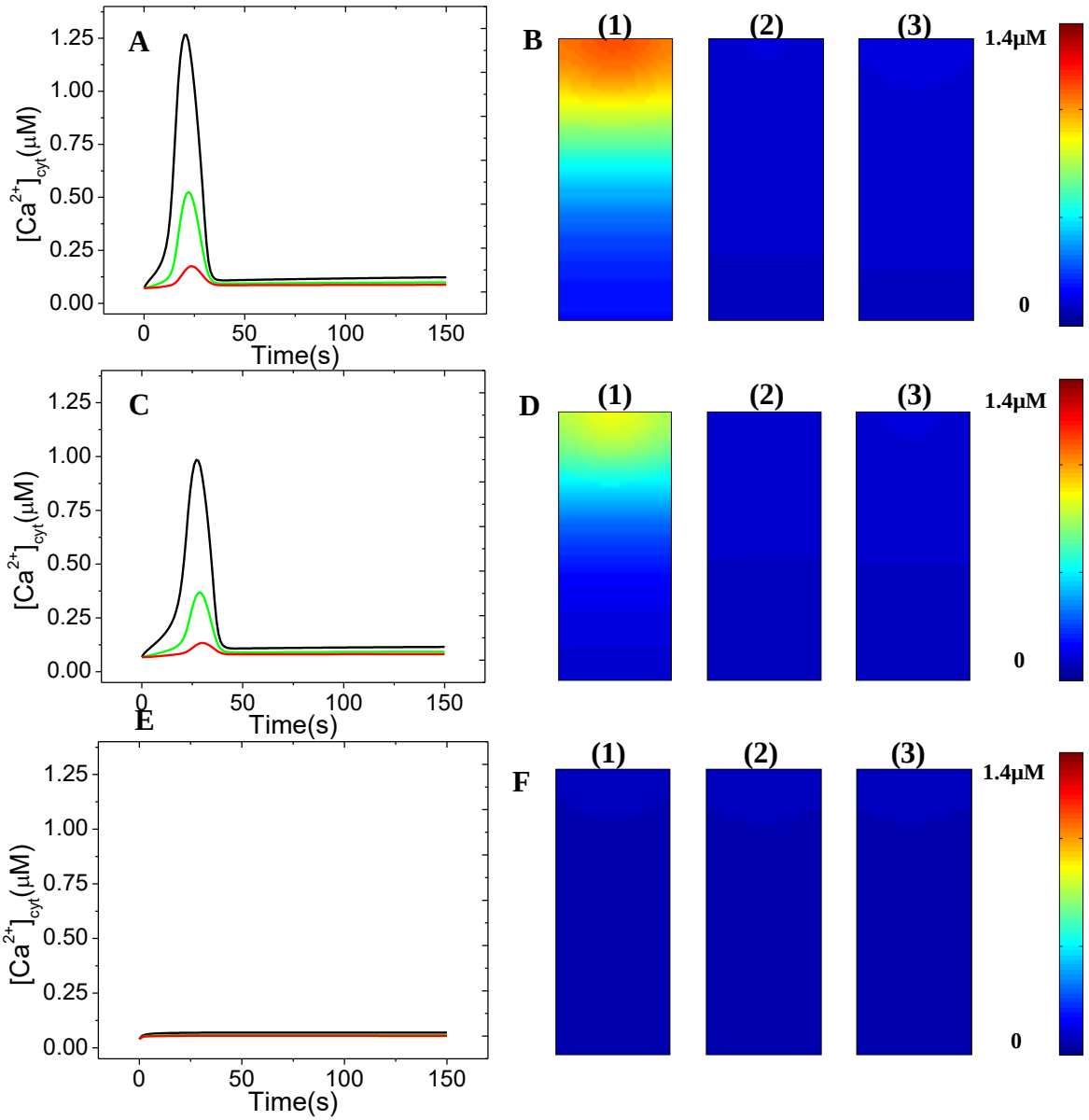

Figure 4.10: (Graphs in the left) Evolution of $[Ca^{2+}]$ at the upper (invasion site)(black), medium (green) and lower point (red) in eqs 3.25-3.29 and the parameter values in table 1, except for V_b and k_1, whose values are, respectively, 0.01μM/s and $0.1s^{-1}$, considering Ca^{2+} and IP_3 diffusion in the cytosol, with all the conditions caused by the bacterium in the invasion site for the next cases: **(A)** normal extracellular Ca^{2+} entry conditions **(C)** Blocking ROCC; **(E)** Blocking SOCC. (Coloured maps in the right and relation to the graphs) Simulated levels of cytosolic Ca^{2+} at 25 (1), 50 (2) and 75s (3) after onset of bacterial invasion depicted in color scale with dark blue and red corresponding to 0 and 1.4μM, respectively, for **(B)** normal extracellular Ca^{2+} entry conditions; **(D)** blocking ROCC; **(F)** blocking SOCC. For $D_I = 10\mu m^2/s$, without diffusion of Ca^{2+} in the ER.

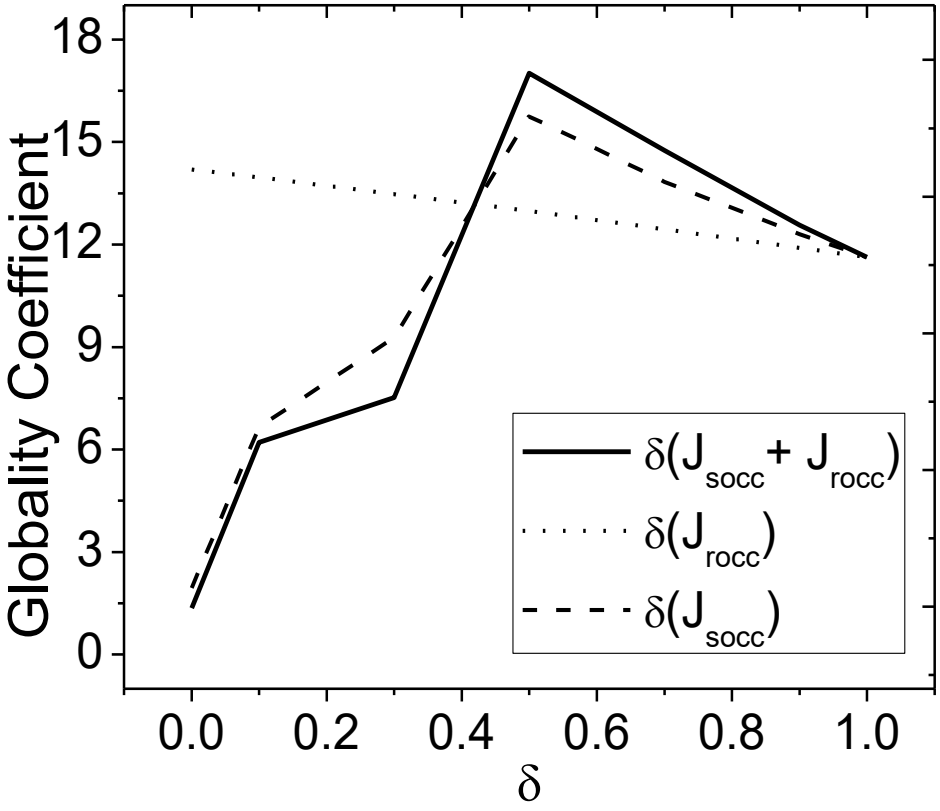

Figure 4.11: Globality coefficient considering $D_I = 10\mu m^2/s$ and without diffusion of Ca^{2+}in the ER

As can be seen in fig. **4.10**, only by blocking SOCC seems to avoid the occurrence of RATPs, while blocking ROCC only seems to produce a lower RATP, supporting the suggestion that that SOCC is much more relevant than ROCC in the responses caused by *Shigella*. Fig. **F.3** shows that, partially blocking ROCC (figs. **F.3A-C)** causes only a small decrease in the $[Ca^{2+}]$ in every part of the cell, while partially blocking SOCC (figs. **F.3D-F)** seems to abruptly decrease the responses between $\delta_{socc} = 0.5$ and $\delta_{socc} = 0.7$ (in contrast with cases I and II, in which the decrease is more gradual) until RATP is avoided.

4.2.2.4 Scenario IV: Slow IP_3 diffusion, with diffusion of Ca^{2+} in the ER

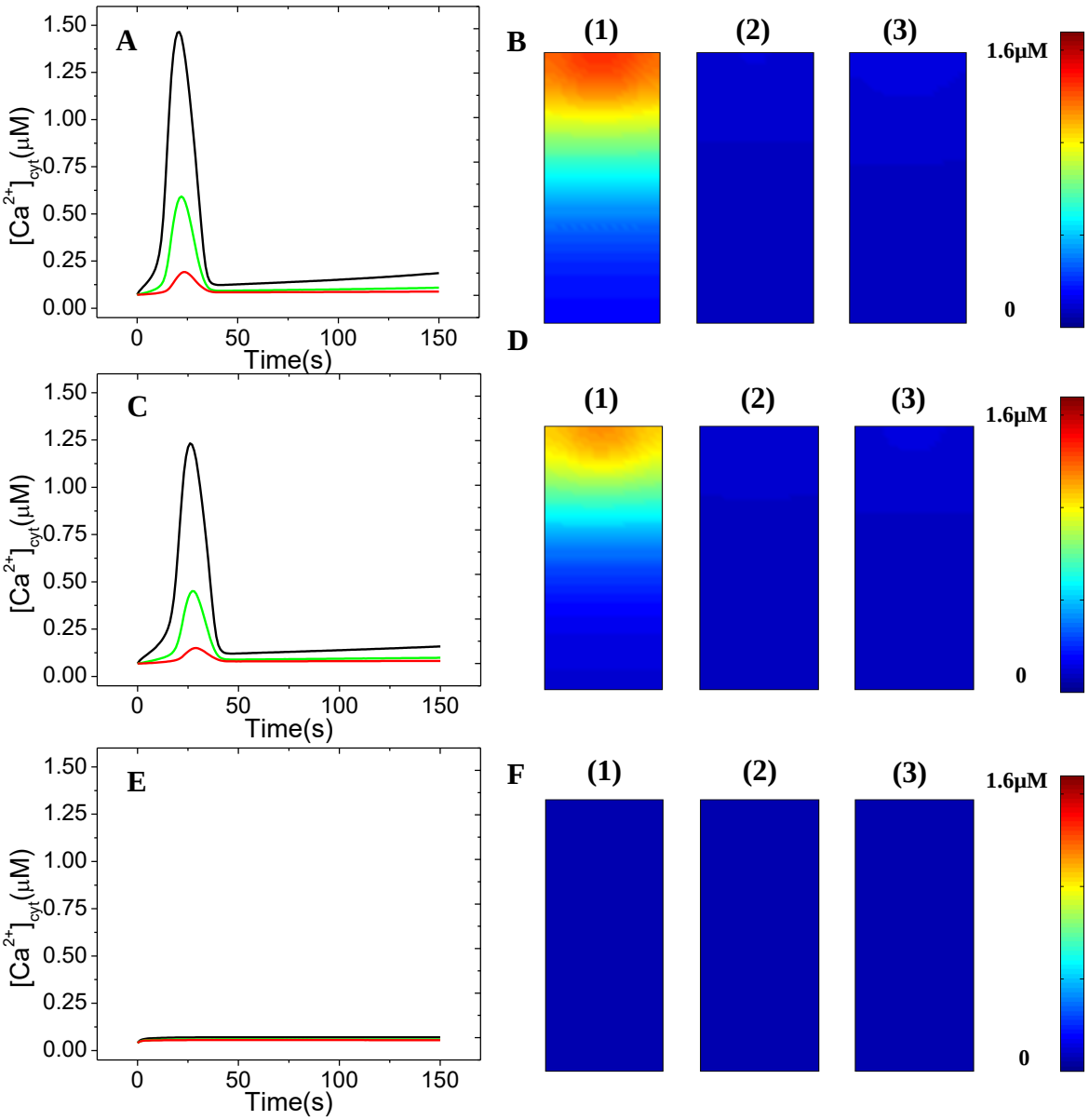

Figure 4.12: (Graphs in the left) Evolution of $[Ca^{2+}]$ at the upper (invasion site)(black), medium (green) and lower point (red) in eqs 3.25-3.29 and the parameter values in table 1, except for V_b and k_1, whose values are, respectively, 0.01μM/s and $0.1s^{-1}$, considering Ca^{2+} and IP_3 diffusion in the cytosol, with all the conditions caused by the bacterium in the invasion site for the next cases: **(A)** normal extracellular Ca^{2+} entry conditions **(C)** Blocking ROCC; **(E)** Blocking SOCC. (Coloured maps in the right and relation to the graphs) Simulated levels of cytosolic Ca^{2+} at 25 (1), 50 (2) and 75s (3) after onset of bacterial invasion depicted in color scale with dark blue and red corresponding to 0 and 1.6μM, respectively, for **(B)** normal extracellular Ca^{2+} entry conditions; **(D)** blocking ROCC; **(F)** blocking SOCC. For $D_I = 10\mu m^2/s$, considering diffusion of Ca^{2+} in the ER.

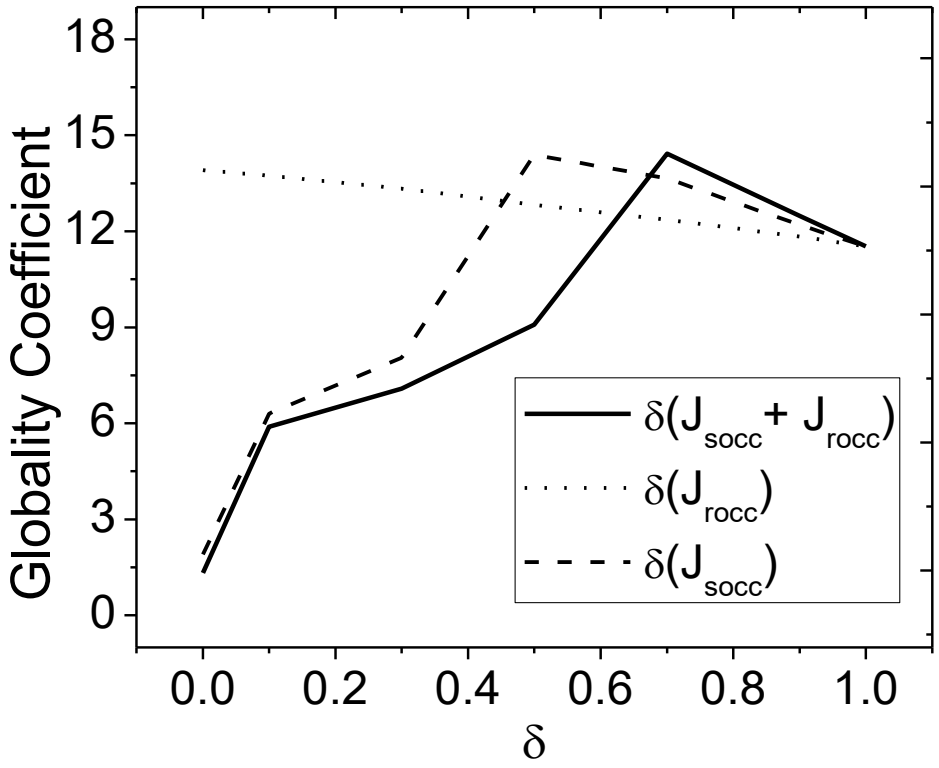

Figure 4.13: Globality coefficient considering $D_I = 10\mu m^2/s$ and with diffusion of Ca^{2+}in the ER

Considering calcium diffusion in the ER gives the same general results as scenario III, with the exception (and in contrast with the comparison between scenario II and I) that for this case, the levels of [Ca^{2+}] are higher than those observed in scenario III.

4.2.3 Discussion of the spatio-temporal simulations considering conditions caused by *Shigella* invasion

The model that we are proposing is built from a selection of previously for previously proposed kinetic expressions for the fluxes and reaction rates, especially from the studies of Dupont and Swillens (1996) and Croisier *et al*. (2013). The model also considers the non-homogeneities in some parameters caused by *Shigella*, reported by Tran Van Nhieu *et al*. (2013) and Sun *et al*. (2017), as well as Ca^{2+} coming from the extracellular space via ROCC and SOCC channels, which have demonstrated to be crucial for the maintaining and control of the frequency of calcium oscillations, particularly SOCC (Croisier *et al*, 2013; Hong *et al*., 2011; Pan, *et al*, 2012).

This model reproduces the previously published data regarding calcium responses during *Shigella* invasion: (1) long-lasting calcium responses produced by *Shigella* at entry sites (RATPs) and (2) elevation of basal cytosolic Ca^{2+} and IP_3 concentrations in the absence of restricted diffusion at entry sites.

We found out in our simulations that SOCC has a more crucial role in Ca^{2+} responses caused by *Shigella* than ROCC, in agreement with experimental data (Croisier *et al*, 2013; Hong *et al*., 2011; Pan, *et al*, 2012). This implies that SOCC thus play an important role as a pharmacological target in order to limit the dispersion of the bacterium in the epithelial tissue. The relevance of SOCC in *Shigella* invasion could be explained by the non-homogeneities induced by the bacterium in the invasion site (an accumulation of IPRs, a greater synthesis of IP_3, as well as a restricted diffusion for cytosolic Ca^{2+} and IP_3); these may cause a greater opening probability for IPRs followed by a depletion of

Ca^{2+} in the ER in the invasion area, leading to a greater activation of SOCC channels, which may thus be necessary to maintain RATPs caused by *Shigella*.

The simulations of Ca^{2+} dynamics during *Shigella* invasion with or without Ca^{2+} diffusion in the ER provided the same general result. This is not a surprise the coefficient diffusion of Ca^{2+} in the ER is three times slower than in the cytosol. However, a decrease in the diffusion coefficient of IP_3 is to $10\mu m^2/s$ caused responses much more local than the default value of this parameter ($280\mu m^2/s$). A lower IP_3 diffusivity is thus in better agreement with experimental results reported by Tran Van Nhieu, *et al* (2013).

The coefficient impacts as well the influence of SOCC: with a high IP_3 diffusion, the globality coefficient decreases when the plasma membrane channels activity is reduced. With a low IP_3 diffusion, the globality coefficient first increases then decreases with a diminution of SOCC. This implies that SOCC channels are in part responsible for the transition from a local to a global response.

Chapter 5

Conclusions and perspectives

5.1 Conclusion

The simulations of the well-mixed model (eqs. 3.14-3.18) show the importance of the inclusion of SOCC, specially for cases in which the synthesis of IP_3 is high, which has been observed in invasion sites, during *Shigella* invasion (Tran Van Nhieu *et al*, 2013). The model proposed in the present thesis is capable to reproduce the following facts reported in literature:

1. Ca^{2+} oscillations in physiological levels (Dupont, G. *et al*., 2017)
2. Contraphase between [Ca^{2+}] in the cytosol and in the endoplasmic reticulum (RE) (Ishii *et al*, 2007)
3. Decrease in the period of oscillations with respect to a greater presence of IP_3 in the cytosol.
4. Lower concentration in the ER as IP_3 synthesis increases (Hattori & Mikoshiba (2000)) g
5. Greater activation of the fraction of STIM proteins linked to ORAI proteins as the synthesis of InP_3 increases.
6. Increase in the period of Ca^{2+} oscillations in the absence of Ca^{2+} flux from the extracellular medium to the cytosol (Ishii *et al*, 2007).

The analysis of the bifurcation and period diagrams shows the relevance of plasma membrane channels (SOCC and ROCC) on the intracellular Ca^{2+} homeostasis and suggests that SOCC could have more relevance than ROCC in the shaping of Ca^{2+}

oscillations. Thus, this supports that SOCC could be crucial in the modulation or mediation of important physiological processes.

Consequently, the results considering a well-mixed cell model give us an idea of how plasma membrane channels, particularly SOCC, can change the behavior of Ca^{2+} responses under different conditions.

To simulate the atypical Ca^{2+} responses induced by *Shigella*, non-homogeneities in some parameters need to be considered, as well as diffusion of Ca^{2+} in the cytosol and in the ER, and of IP_3 in the cytosol, which were all considered using a Fickian Diffusion approach.

In the results regarding bacterial invasion the following can be concluded:

1. For the cases regarding fast IP_3 diffusion, the reduction of SOCC activity seems to cause a more global response than partially blocking ROCC.
2. For the cases considering slow IP_3 diffusion, SOCC seems to be determinant in the local/global character of the reponses.
3. SOCC seems to avoid RATPs to occur in the four cases that we considered.
4. Partially blocking all the plasma membrane channels could provide a way to play with the local/global response in order to limit bacterial dissemination (as can be seen in cases III IV); for example, causing a faster cellular death by making the responses more global to limit bacterial invasion or avoiding RATPs to occur.

5.2 Perspectives

- To develop a mathematical model to analyse the intercellular Ca^{2+} responses induced by *Shigella* invasion in a group of epithelial cells, using paracrine secretion.
- To develop a Gillespie's Algorithm (See Appendix A) of the model of Ca^{2+} responses induced by *Shigella* in order to take the molecular noise introduced by plasma membrane channels into account.
- To extend the model to 3-dimensions, considering a more realistic geometry of epithelial cells.
- To simulate the model using the Finite Element technique in order to consider a more realistic geometry of the ER.
- To simulate the model considering anomalous subdiffusion, which have been demonstrated to give better approximations than Fickian diffusion when modelling Ca^{2+} waves (Tan *et al*., 2007)

Appendix A

Stochastic version of the well-mixed cell model

Even though intracellular Ca^{2+} whole-cell behavior can be described by mean field differential equations, it is well known that at the sub-cellular level Ca^{2+} dynamics are governed by stochasticity. Inherent to stochasticity, molecular noise arises from the low number of molecules of biochemical reactions in the cell (Gonze, D. *et al*, 2018).

Since it has been demonstrated that SOCCs play an important role in a variety of cellular processes, including proliferation, apoptosis, gene transcription and motility, the noise produced by this channels must have important physiological consequences, making the study of SOCCs interesting from a stochastic perspective.

The Gillespie algorithm is a standard and rigorous way to simulate stochastic (bio)chemical systems (Gillespie, D., 1977) and is suitable for studying the molecular noise in biological systems. It considers a certain propensity associated to each individual reaction. These propensities can be derived from the macroscopic kinetic rates and can be converted into probabilities.

To obtain the stochastic version of the well-mixed cell model, described by equations 3,14-3,18, it has to be converted into a reaction scheme, adapting the 5 variables of the system to number of molecules, IP_3 receptors and Store-Operated channels.

The propensities for the reaction scheme based on equations 3.14-3.18 are the following,

$$\omega_1 = \alpha_1 I \tag{A.1}$$

$$\omega_2 = \left(V_s\right)\left(\Omega_{cyt}\right)P_{so} \tag{A.2}$$

$$\omega_3 = \alpha k_1\left(b\right)\left(c_s - C\right) \tag{A.3}$$

$$\omega_4 = \alpha k_1\left((1-R_i)\frac{I}{K+I}\frac{C^{na}}{K_A^{na}+C^{na}}\right)\left(c_s - C\right) \tag{A.4}$$

$$\omega_5 = V_e\frac{C^2}{K_e^2+C^2} \tag{A.5}$$

$$\omega_6 = V_p\frac{C^2}{K_p^2+C^2} \tag{A.6}$$

$$\omega_7 = V_b \tag{A.7}$$

$$\omega_8 = k_d I \tag{A.8}$$

$$\omega_9 = k_+\left(1-R_i\right)\frac{C^{ni}}{1+\left(\frac{C}{K_A}\right)^{na}} \tag{A.9}$$

$$\omega_{10} = k_- R_i \tag{A.10}$$

$$\omega_{11} = \left(\frac{K_s^4}{K_s^4+c_s^4}\right)/\tau_s \tag{A.11}$$

$$\omega_{12} = P_{so}/\tau_s \tag{A.12}$$

Table A.1: Stochastic version of the system described by equations 3.14-3.18. In this version, the variables are expressed in numbers of molecules and open channels. The nomenclature is adapted as follows: $x_1 = C, x_2 = c_s, x_3 = I, x_4 = R_i \; and \; x_5 = P_{so}$. Parameter values have thus to be adapted.

No	*Reaction*	*Propensities*	*Stoichiometric Coefficients*	*No*	*Reaction*	*Propensities*	*Stoichiometric Coefficients*
1	$\rightarrow x_1$	ω_1	$\eta_{11} = 1$	7	$x_3 \rightarrow$	ω_7	$\eta_{37} = -1$
2	$\rightarrow x_1$	ω_2	$\eta_{12} = 1$	8	$\rightarrow x_4$	ω_8	$\eta_{48} = 1$
3	$x_2 \rightarrow x_1$	ω_3	$\eta_{13} = 1$ $\eta_{23} = -1$	9	$x_4 \rightarrow$	ω_{10}	$\eta_{49} = -1$
4	$x_2 \rightarrow x_1$	ω_4	$\eta_{14} = 1$ $\eta_{24} = -1$	10	$x_4 \rightarrow$	ω_{10}	$\eta_{410} = -1$
5	$x_1 \rightarrow x_2$	ω_5	$\eta_{15} = -1$ $\eta_{25} = 1$	11	$\rightarrow x_5$	ω_{11}	$\eta_{511} = 1$
6	$x_1 \rightarrow x_2$	ω_6	$\eta_{16} = -1$ $\eta_{26} = 1$	12	$x_5 \rightarrow$	ω_{12}	$\eta_{512} = -1$

In order to adapt the nomenclature from deterministic to stochastic, the variables C, c_s, I, R_i and Pso are converted to interacting species x_1, x_2, x_3, x_4 and x_5, respectively, which are involved in M reactions: R_1, R_2,..., R_M, with corresponding reaction propensities.

The deterministic values of the concentrations have to be adapted to number of molecules by means of the parameter Ω, as well as the IPRs, which are scaled with R_t, whose values are 10^5 and 6000 (Sun *et al*., 2017), respectively. To run the simulations shown in figure A.2, the fraction of open STIM/Orai proteins (Pso) has to be scaled to total number of Stim/ORAI channels with a parameter, which we will call P_t and whose value has not been reported in literature.

To estimate P_t we use the Gillespie Algorithm to simulate the time evolution of the system for different P_t values, considering a large number of molecules, until we observe a similar time-course as the deterministic approach. The value of P_t that we estimate is equal to 1000.

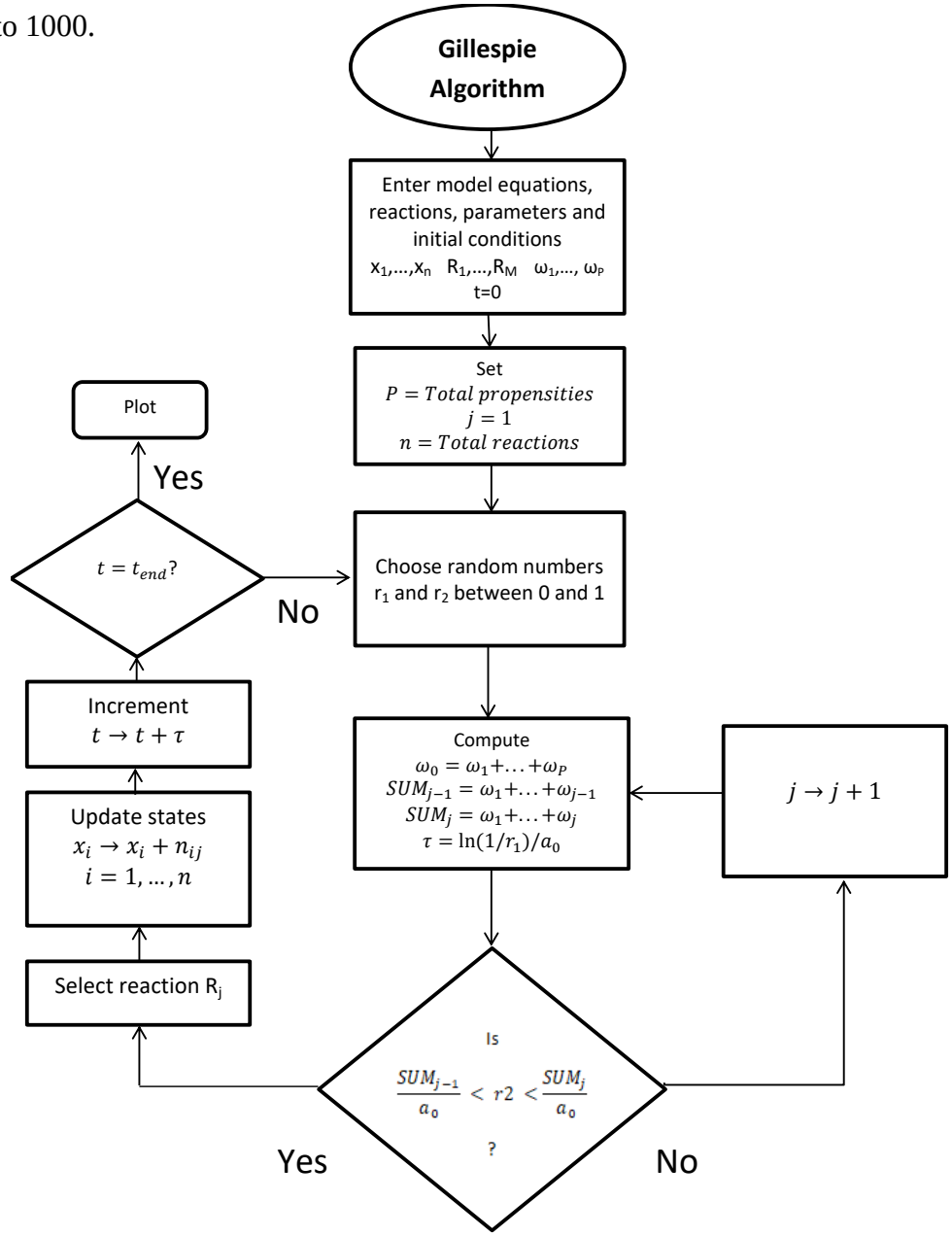

Figure A.1: Gillespie Algorithm flowchart

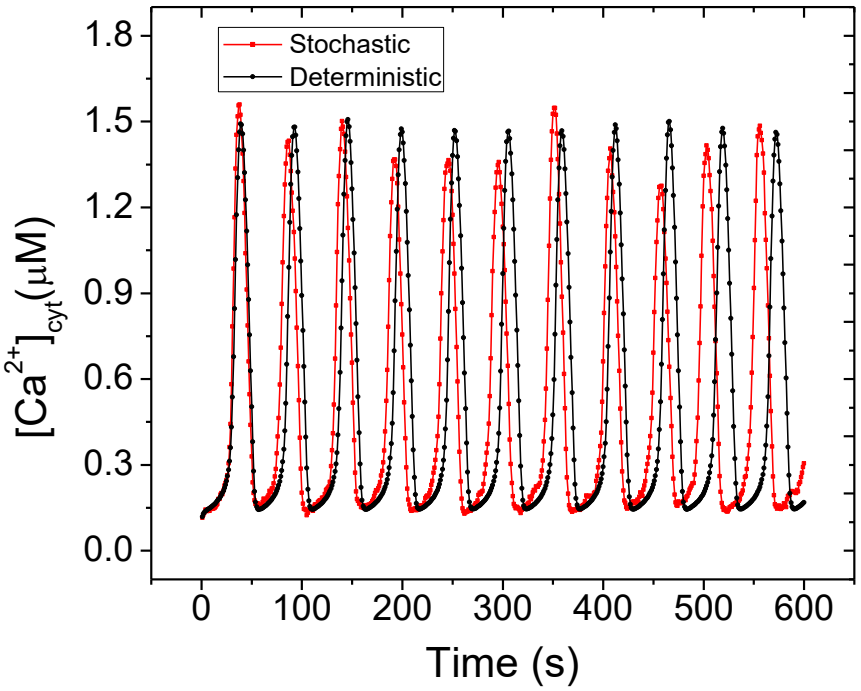

Figure A.2*: Deterministic (black) and stochastic (red) simulations using parameters from table 3.1 and* $\Omega = 10000$, $R_t = 6000$ *and* $P_t = 1000$ *considering the stochastic approach.*

Appendix B

Research products during the master

[1] Ornelas G. Roberto, Wacquier Benjamin, Dupont Geneviève, González-Velez Virginia (2018). Modelling the cytosolic [Ca^{2+}] responses induced by *Shigella* invasion in epithelial cells. Oral presentation at the International Conference on Innovation in Bioinformatics and Biomedical Engineering, ICIBBE 2018. Barcelona, España.

Appendix C

Finite difference formulation for the diffusive functions

The finite difference formulation of the diffusive terms in equations 3.25-3.27 were obtained as follows.

The first step is to expand the concentration functions using Taylor series in the positions x+Δx and x-Δx around the values of the function, and their derivatives in the position x

$$C(x+\Delta x)=C(x)+\Delta x\frac{dC}{dx}\bigg|_x+\frac{(\Delta x)^2}{2!}\frac{d^2C}{dx^2}\bigg|_x+\frac{(\Delta x)^3}{3!}\frac{d^3C}{dx^3}\bigg|_x+\frac{(\Delta x)^4}{4!}\frac{d^4C}{dx^4}\bigg|_x+\ldots \quad \text{(C.13)}$$

$$C(x-\Delta x)=C(x)+(-\Delta x)\frac{dC}{dx}\bigg|_x+\frac{(-\Delta x)^2}{2!}\frac{d^2C}{dx^2}\bigg|_x+\frac{(-\Delta x)^3}{3!}\frac{d^3C}{dx^3}\bigg|_x+\frac{(-\Delta x)^4}{4!}\frac{d^4C}{dx^4}\bigg|_x+\ldots \quad \text{(C.14)}$$

To discretise the differential equations describing the diffusion of the concentration, a representation of the second derivative must be found. To do that, equation C.1 must be added to equation C.2 to obtain

$$C(x+\Delta x)+C(x-\Delta x)=2C(x)+(\Delta x)^2\frac{d^2C}{dx^2}\bigg|_x+\frac{1}{12}(\Delta x)^4\frac{d^4C}{dx^4}\bigg|_x+\ldots \quad \text{(C.15)}$$

Reorganising C.3

$$\frac{d^2C}{dx^2}\bigg|_x=\frac{C(x+\Delta x)-2C(x)+C(x-\Delta x)}{(\Delta x)^2}+\frac{1}{12}(\Delta x)^4\frac{d^4C}{dx^4}\bigg|_x+\ldots \quad \text{(C.16)}$$

Which can be written as

$$\frac{d^2C}{dx^2}\bigg|_x=\frac{C(x+\Delta x)-2C(x)+C(x-\Delta x)}{(\Delta x)^2}+\mathrm{O}\left[(\Delta x)^2\right] \quad \text{(C.17)}$$

Where the symbol O represents the order of magnitude of the last term in C.4. Neglecting the term $O\left[\left(\Delta x\right)^2\right]$ in C.5, we obtain the approximation of the second derivative

$$\left.\frac{d^2C}{dx^2}\right|_x \cong \frac{C(x+\Delta x)-2C(x)+C(x-\Delta x)}{\left(\Delta x\right)^2} \tag{C.18}$$

The same is applicable for the deduction of finite differences in the *y* coordinate and for the terms describing diffusion of Ca^{2+} in the ER and diffusion of IP_3 in the cytosol, which gives us,

$$\left.\frac{d^2C}{dx^2}\right|_x + \left.\frac{d^2C}{dy^2}\right|_y \cong \frac{C(x+\Delta x)-2C(x)+C(x-\Delta x)}{\left(\Delta x\right)^2} + \frac{C(y+\Delta y)-2C(y)+C(y-\Delta y)}{\left(\Delta y\right)^2} \tag{C.19}$$

$$\left.\frac{d^2c_s}{dx^2}\right|_x + \left.\frac{d^2c_s}{dy^2}\right|_y \cong \frac{c_s(x+\Delta x)-2c_s(x)+c_s(x-\Delta x)}{\left(\Delta x\right)^2} + \frac{c_s(y+\Delta y)-2c_s(y)+c_s(y-\Delta y)}{\left(\Delta y\right)^2} \tag{C.20}$$

$$\left.\frac{d^2I}{dx^2}\right|_x + \left.\frac{d^2I}{dy^2}\right|_y \cong \frac{I(x+\Delta x)-2I(x)+I(x-\Delta x)}{\left(\Delta x\right)^2} + \frac{I(y+\Delta y)-2I(y)+I(y-\Delta y)}{\left(\Delta y\right)^2} \tag{C.21}$$

Expressing equations C.7-C.9 in indicial notation, considering the index i and j for *x* and *y* respectively, gives

$$\frac{d^2C}{dx^2} + \frac{d^2C}{dy^2} \cong \frac{C_{i+1,j}-2C_{i,j}+C_{i-1,j}}{\left(\Delta x\right)^2} + \frac{C_{i,j+1}-2C_{i,j}+C_{i,j-1}}{\left(\Delta y\right)^2} \tag{C.22}$$

$$\frac{d^2c_s}{dx^2} + \frac{d^2c_s}{dy^2} \cong \frac{c_{s_{i+1,j}}-2c_{s_{i,j}}+c_{s_{i-1,j}}}{\left(\Delta x\right)^2} + \frac{c_{s_{i,j+1}}-2c_{s_{i,j}}+c_{s_{i,j-1}}}{\left(\Delta y\right)^2} \tag{C.23}$$

$$\frac{d^2I}{dx^2}+\frac{d^2I}{dy^2}\cong\frac{I_{i+1,j}-2I_{i,j}+I_{i-1,j}}{\left(\Delta x\right)^2}+\frac{I_{i,j+1}-2I_{i,j}+I_{i,j-1}}{\left(\Delta y\right)^2} \quad \text{(C.24)}$$

The diffusive terms describing C, Cs and I, considering $\Delta x=\Delta y$, $M_C=D_C/\left(\Delta x\right)^2$, $M_I=D_I/\left(\Delta x\right)^2$ and $M_{c_s}=D_{c_s}/\left(\Delta x\right)^2$, can be expressed as diffusive funcitions (Ψ_{C}, Ψ_{c_s} and Ψ_I) depending on the discretised concentrations in the position (i,j), which gives

$$\Psi_{\mathrm{C}}(C_{i,j})=M_C(C_{i-1,j}+C_{i+1,j}-4C_{i,j}+C_{i,j+1}+C_{i,j-1}) \quad \text{(C.25)}$$

$$\Psi_{\mathrm{I}}(I_{i,j})=M_I(I_{i-1,j}+I_{i+1,j}-4I_{i,j}+I_{i,j+1}+I_{i,j-1}) \quad \text{(C.26)}$$

$$\Psi_{c_s}(c_{s_{(i,j)}})=M_{c_s}(c_{s_{(i-1,j)}}+c_{s_{(i+1,j)}}-4c_{s_{(i,j)}}+c_{s_{(i,j+1)}}+c_{s_{(i,j-1)}}) \quad \text{(C.27)}$$

Appendix D

Glossary

Actin-cytoskeleton. The actin cytoskeleton is a complex network of polarized filaments that is involved in many essential processes including motility and cytokinesis, tumor cell transformation and metastasis.

Agonist. An agonist is a compound that can bind to and cause activation of a receptor, thus mimicking an endogenous ligand or neurotransmitter.

Apoptosis. Programmed cell death.

Ca^{2+}-induced Ca^{2+} release (CICR). The autocatalytic release of Ca^{2+} from the endoplasmic or sarcoplasmic reticulum through IP3 receptors or ryanodine receptors. CICR causes the fast release of large amounts of Ca^{2+} from internal stores and is the basis for Ca^{2+} oscillations and waves in a wide variety of cell types.

G Protein Coupled Recepor (GPCR). A receptor in the cell membrane that converts an extracellular signal into an intracellular signal via coupling to G proteins.

Global response. Calcium increase that spread in the whole invaded cell.

Inositol-trisphosphate Receptor (IPR). Proteins in the membrane of the endoplasmic/sarcoplasmic reticulum that bind IP3, leading to the release of Ca2+ from the ER/SR.

Inositol 1,4,5-trisphosphate (IP_3). A second messenger responsible for the release of intracelular Ca^{2+} from internal stores, through IP_3 receptors.

Receptor-Operated Calcium Channel (ROCC). Membrane Ca^{2+} channels that are opened, not by depletion of the internal Ca^{2+} stores, but indirectly by the activated G-protein-coupled receptor. The molecular identity of ROCC remains unclear, but they are often activated by IP_3.

Responses Associated with Trespassing Pathogens (RATPs). Local calcium responses lasting more than 5 seconds.

Sarco/Endoplasmic Ca^{2+} ATPase (SERCA). A Ca^{2+} ATPase pump that transports Ca^{2+} up its concentration gradient from the cytoplasm to the ER/SR.

Second messenger. Second messengers are the key distributors of an external signal, as they are released into the cytosol as a consequence of receptor activation and are responsible for affecting a wide variety of intracellular enzymes, ion channels and transporters.

Stromal Interaction Molecule (STIM). A protein, situated in the ER/SR membrane, that senses depletion of Ca^{2+} in the ER/SR.

Store-Operated Calcium Channel (SOCC). Membrane Ca^{2+} channels that are opened by depletion of the $[Ca^{2+}]$ in the ER/SR. In many cell types (but probably not all), SOCC are Orai channels that have been activated by STIM.

Transient Receptor Potential (canonical) channels (TRP). A large family of membrane Ca^{2+} channels (although not specific to Ca^{2+}) that are regulated by a variety of molecules, including arachidonic acid. TRPC channels are thought to form receptor-operated Ca^{2+} channels, but may also be involved in store-operated Ca^{2+} entry.

Type III Secretion System (T3SS). Complex macromolecular machines that have evolved to subvert host cell function through the translocation of virulence proteins directly from the bacterial cytoplasm into the host cell.

Orai. A class of membrane Ca^{2+} channels that are encoded by the orai genes (with three homologs; Orai1, Orai2, and Orai3). Orai channels interact with STIM proteins, which are themselves activated by depletion of Ca^{2+} in the ER. Thus, Orai channels are a principal component of store operated Ca^{2+} entry

Phospholipase C (PLC). The enzyme that splits PIP2 into DAG and IP3. There are 13 kinds of PLC, classified into 6 iso-types, and they are mostly activated by G-protein-coupled receptors.

Plasma Membrane Ca^{2+} ATPase (PMCA). A membrane ATPase Ca^{2+} pump that removes Ca^{2+} from the cell.

Local response. Calcium transient localised in the invasion area.

Appendix E

Swillens's Model for IPRs

The model for IPRs proposed by Swillens, *et al.* (1994) is based on the next generally accepted hypothesis.

1. Ca^{2+} may bind to the IPR at distinct activating or inbibitory sites. Binding to them is mutually exclusive. Three forms of receptor therefore exist, R, R_a and R_i, with an affinity that we assume the same for all three forms (IR, IR_a, IR_i).
2. The channel may open only if it is in the IR_a state. With Ca^{2+} bound to the inhibitory site (R_i, IR_i), the channel is desensitized.
3. Binding of IP_3 and Ca^{2+} to the activating site are always at equilibrium, but binding of Ca^{2+} to the inhibitory site develops slowly.
4. The IP_3-controlled gate is situated on the transmembrane part of the channel. The Ca^{2+}-binding sites are located in an intermediate compartment defined downstream from the gate along the permeation pathway. This compartment is considered as a macroscopic domain in which a homogeneous [Ca^{2+}] is defined (this is obviously an oversimplified but useful description) and is probed by the binding sites.

The slower binding reaction is the Ca^{2+} binding to the inhibiting site. Thus, it is necessary a equation to describe the variation of the fraction of deshinibited receptor with respect to time:

$$\frac{dR_i}{dt} = k_+ \left(1 - R_i\right) \frac{C^{ni}}{1 + \left(\frac{C}{K_A}\right)^{na}} - k_- R_i \qquad \text{(E.1)}$$

In eq. E.1 can be seen that the binding of Ca^{2+} to the activating and inhibitory Ca^{2+}-binding sites is assumed to be cooperative, with aparent equilibrium dissociation constant K_A and Hill coefficients n_a and n_i, were k_+ and k_- are the kinetic constants of Ca^{2+} association to and dissociation from the inhibiting site, respectively.

The fraction of "activatable" receptor is referred to as R_{able}. At any time, this fraction is given by

$$R_{able} = (1 - R_i)\left(\frac{I}{K + I}\right) \tag{E.29}$$

And the fraction of active receptors is given by

$$R_a = \left(\frac{R_{able}}{1 + \frac{K_A^{na}}{C^{na}}}\right) \tag{E.30}$$

Substituting E.2 in E.3 gives:

$$R_a = (1 - R_i)\frac{I}{K + I}\frac{C^{na}}{K_A^{na} + C^{na}} \tag{E.31}$$

Which is the expression that describes the active IPRs.

Appendix F

Partially blocking SOCC and ROCC for Scenarios I-IV

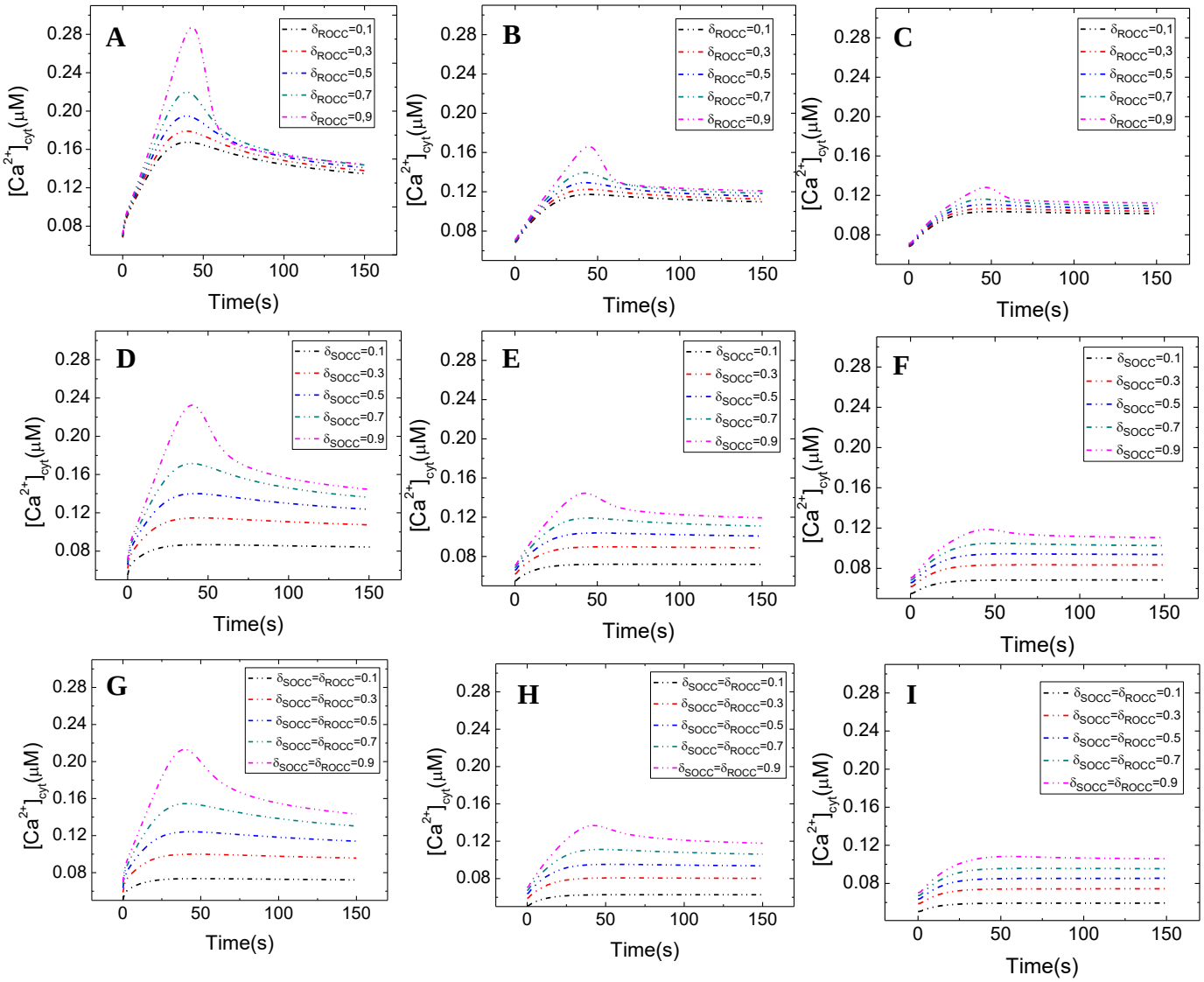

Figure F.1: Evolution of [Ca^{2+}] for the case without Ca^{2+}diffusion in the ER and $D_I = 280\mu m^2/s$ at the upper (invasion site): partially blocking **(A)** J_{ROCC}, **(B)** J_{SOCC} and **(C)** J_{ROCC} and J_{SOCC}; at the medium of the cell: partially blocking **(D)** J_{ROCC}, **(E)** J_{SOCC} and **(F)** J_{ROCC} and J_{SOCC} and lower point: partially blocking **(G)** J_{ROCC}, **(H)** J_{SOCC} and **(I)** J_{ROCC} and J_{SOCC} in eqs 3.25-3.29 and the parameter values in table 1, except for V_b and k_1, whose values are, respectively, 0.01μM/s and $0.1s^{-1}$, considering Ca^{2+} and IP_3 diffusion, with all the conditions caused by the bacterium.

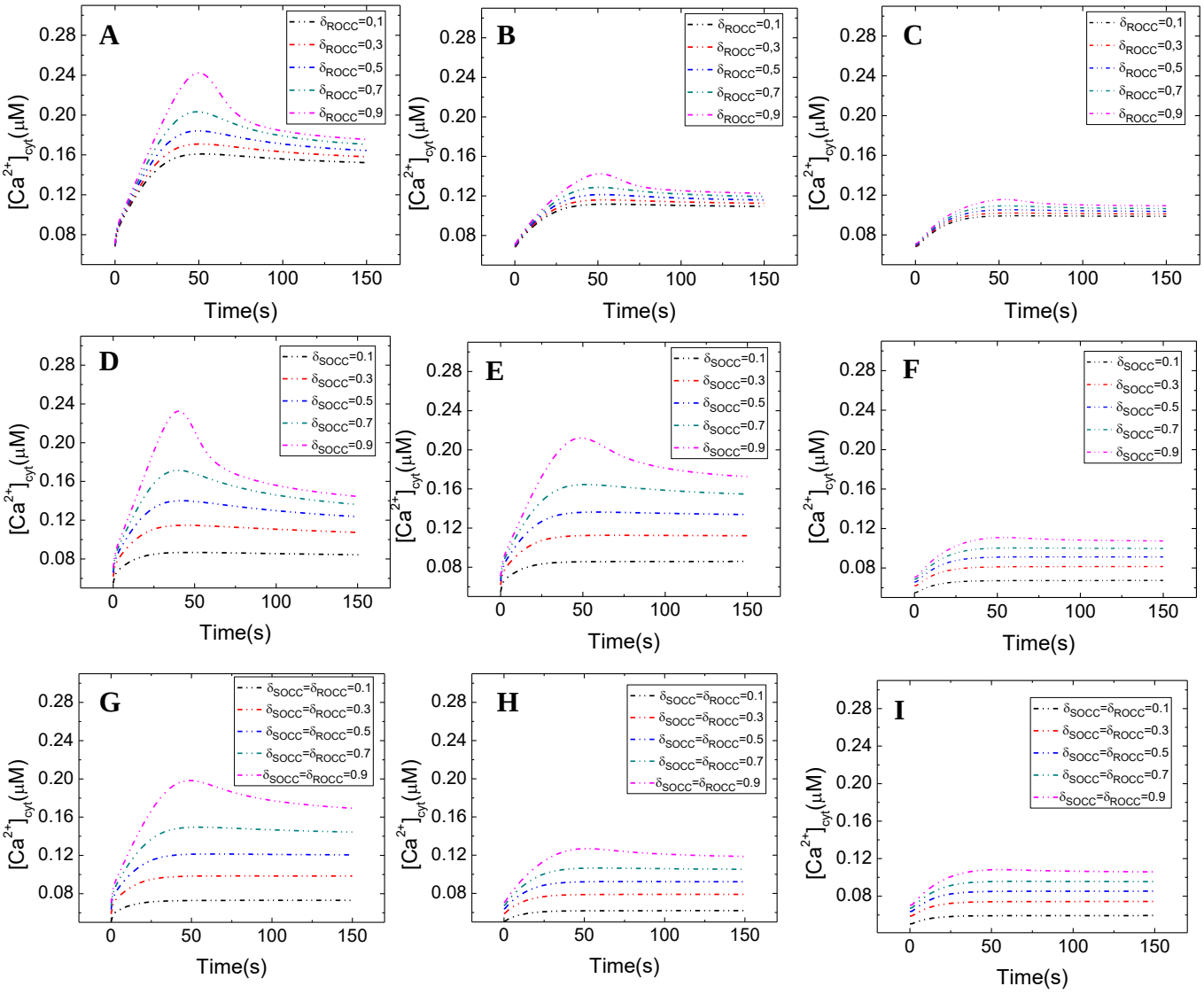

Figure F.2: Evolution of [Ca^{2+}] for the case with Ca^{2+}diffusion in the ER and $D_I = 280\mu m^2/s$ at the upper (invasion site): partially blocking (A) J_{ROCC}, (B) J_{SOCC} and (C) J_{ROCC} and J_{SOCC}; at the medium of the cell: partially blocking (D) J_{ROCC}, (E) J_{SOCC} and (F) J_{ROCC} and J_{SOCC} and lower point: partially blocking (G) J_{ROCC}, (H) J_{SOCC} and (I) J_{ROCC} and J_{SOCC} in eqs 3.25-3.29 and the parameter values in table 1, except for V_b and k_1, whose values are, respectively, 0.01μM/s and $0.1s^{-1}$, considering Ca^{2+} and IP_3 diffusion, with all the conditions caused by the bacterium.

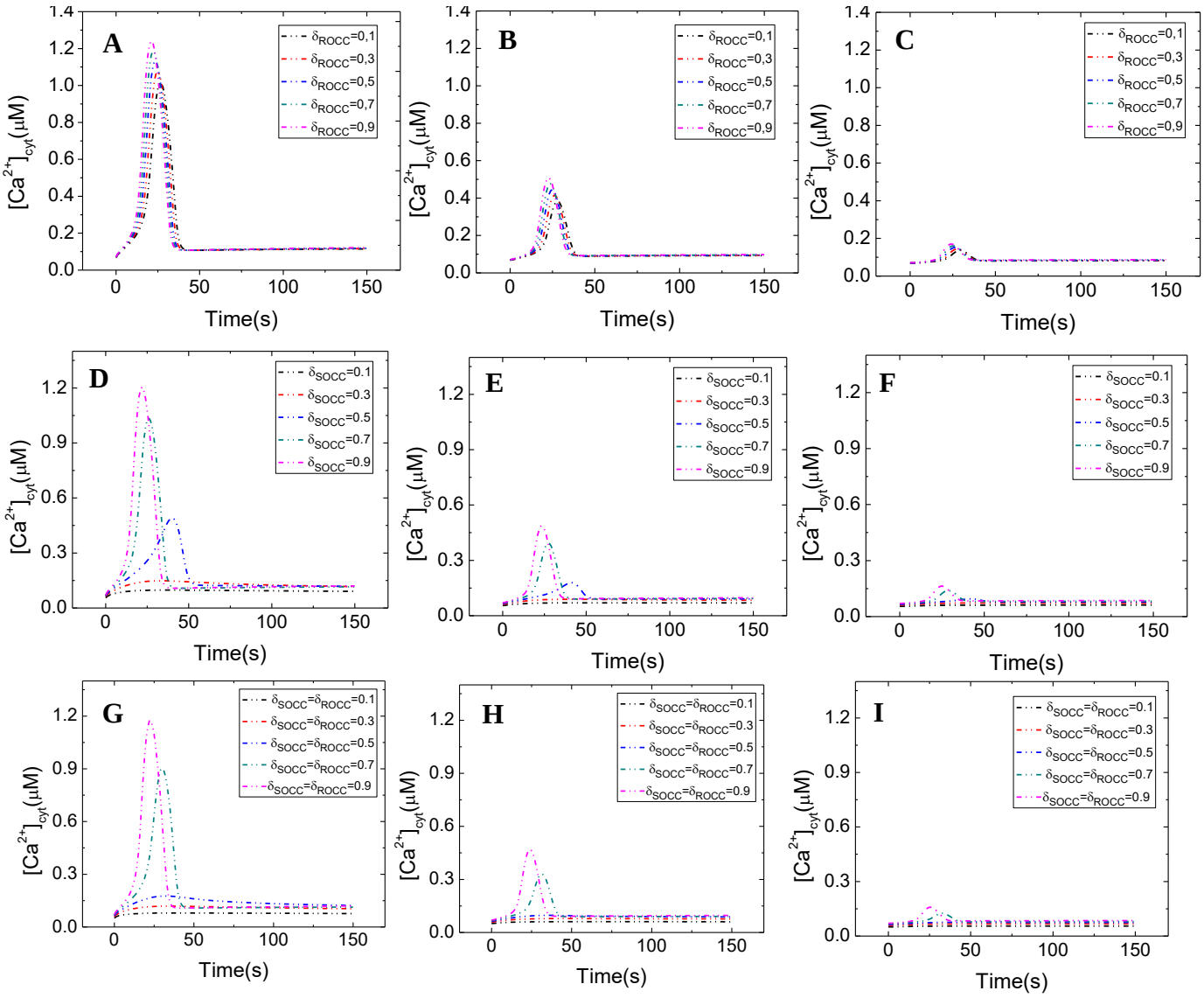

Figure F.3: Evolution of [Ca^{2+}] for the case without Ca^{2+}diffusion in the ER and $D_I = 10\mu m^2/s$ at the upper (invasion site): partially blocking **(A)** J_{ROCC}, **(B)** J_{SOCC} and **(C)** J_{ROCC} and J_{SOCC}; at the medium of the cell: partially blocking **(D)** J_{ROCC}, **(E)** J_{SOCC} and **(F)** J_{ROCC} and J_{SOCC} and lower point: partially blocking **(G)** J_{ROCC}, **(H)** J_{SOCC} and **(I)** J_{ROCC} and J_{SOCC} in eqs 3.25-3.29 and the parameter values in table 1, except for V_b and k_1, whose values are, respectively, 0.01μM/s and $0.1s^{-1}$, considering Ca^{2+} and IP_3 diffusion, with all the conditions caused by the bacterium.

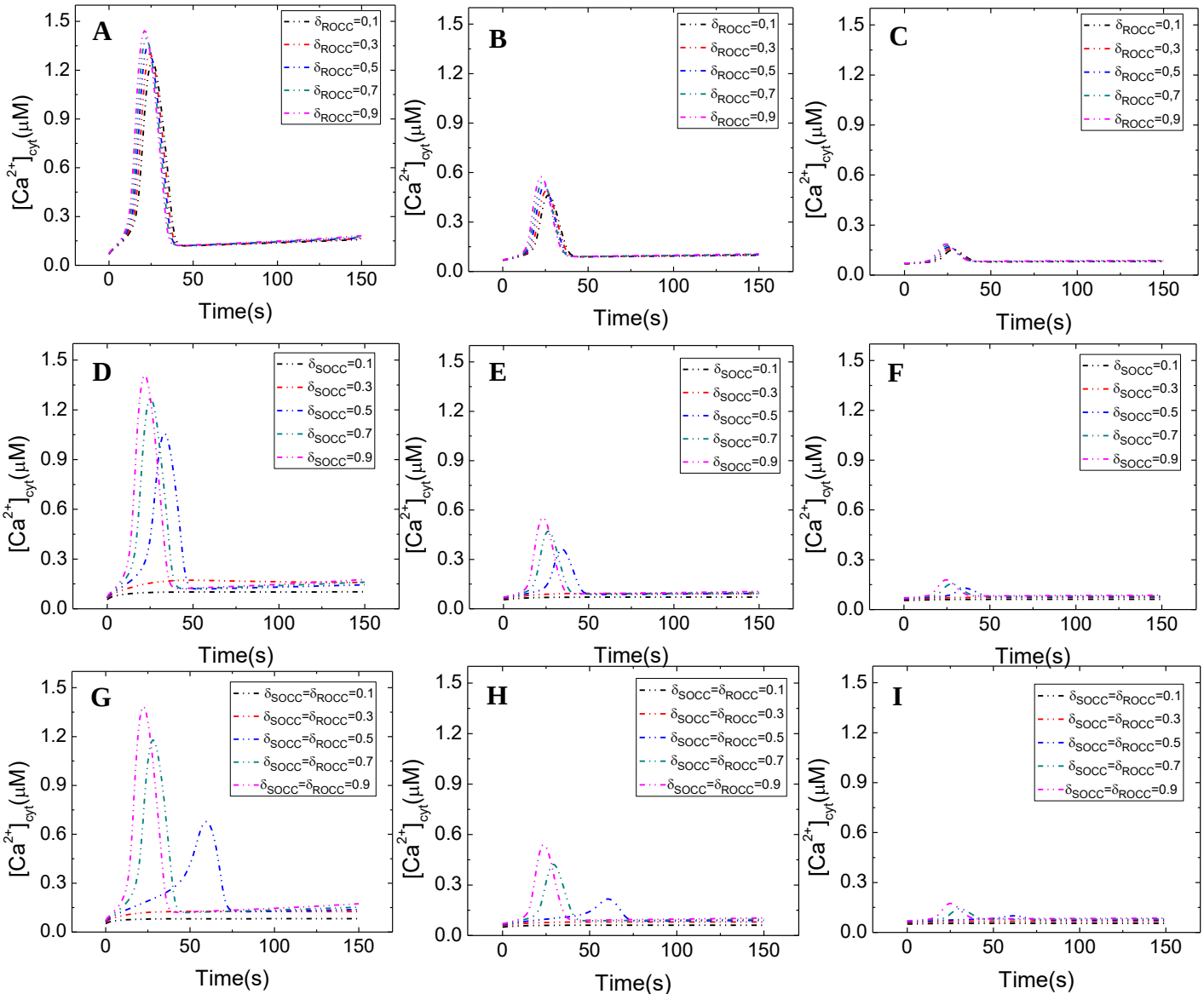

Figure F.4: Evolution of $[Ca^{2+}]$ for the case with Ca^{2+}diffusion in the ER and $D_I = 10\mu m^2/s$ at the upper (invasion site): partially blocking (A) J_{ROCC}, (B) J_{SOCC} and (C) J_{ROCC} and J_{SOCC}; at the medium of the cell: partially blocking (D) J_{ROCC}, (E) J_{SOCC} and (F) J_{ROCC} and J_{SOCC}; at lower point: partially blocking (G) J_{ROCC}, (H) J_{SOCC} and (I) J_{ROCC} and J_{SOCC} in eqs 3.25-3.29 and the parameter values in table 1, except for V_b and k_1, whose values are, respectively, 0.01μM/s and $0.1s^{-1}$, considering Ca^{2+} and IP_3 diffusion, with all the conditions caused by the bacterium.

References

- Bonnet, M. and Tran Van Nhieu, G. (2016) How Shigella Utilizes Ca2+ Jagged Edge Signals during Invasion of Epithelial Cells. Front. Cell. Infect. Microbiol. 6:16.
- Boal F, Puhar A, Xuereb JM, Kunduzova O, Sansonetti PJ, Payrastre B, Tronchere H (2016)PI5P triggers ICAM-1degradation in shigella infected cells, thus dampening immune cell recruitment.Cell Rep14: 750–759
- Bourdet-Sicard, R., Egile, C., Sansonetti, P., Tran Van Nhieu, G. (2000). Diversion of cytoskeletal processes by Shigella during invasion of epithelial cells. Microbes and Infection, 2, 813-819.
- Carayol, N. and Tran Van Nhieu, G.. (2013). Tips and tricks about Shigella invasion of epithelial cells. Current Opinion in Microbiology, 16, 32-37.
- Dupont, G., Falcke, M., Kirk, V. and Sneyd, J. (2017). Models of Calcium Signalling. Switzerland: Springer.
- Dupont, G. & Sneyd, J. (2017). Recent developments in models of calcium signalling. Current opinion in systems biology, 3, 17-22.
- Dupont, G. & Swillens, S. (1996). Quantal release, incremental detection, and longperiod Ca2þoscillations in a model based on regulatory Ca2þ-binding sites along the permeation pathway.Biophys. J.71,1714–1722
- Fall, C., Marland, E., Wagner, J. and Tyson, J. (2000). Computational Cell Biology. New York: Springer.

- Gillespie DT (1976). General method for numerically simulating stochastic time evolution of coupled chemical-reactions.J Comput Phys, 22, 403–434.
- Ishii, K., Hirose, K. & Iino, M. (2007). Ca^{2+} shuttling between endoplasmic reticulum and mitochondria underlying Ca^{2+} oscillations. EMBO report 7,390–396.
- Jenkins, C. (2016). Shigella. Encyclopedia of Food and Health, 785–789.
- Konradt C, Frigimelica E, Nothelfer K, Puhar A, Salgado-Pabon W, di Bartolo V, Scott-Algara D, Rodrigues CD, Sansonetti PJ, Phalipon A (2011) The Shigella flexneritype three secretion system effector IpgD inhibits T cell migration by manipulating host phosphoinositide metabolism. Cell Host Microbe,9, 263–272
- Kowalewski, J., Uhlén, P., Kitano, H. & Brismar, H.. (2006). Modeling the impact of store-operated Ca2+ entry on intracellular Ca2+ oscillations. Mathematical Biosciences, 204, 232-249.
- Luik R, Wang B, Prakriya M, Wu M, Lewis R (2008) Oligomerization of STIM1 couples ER calcium depletion to CRAC channel activation. Nature 454: 538–542
- Lytton J, Westlin M, Burk SE, Shull GE, MacLennan DH (1992) Functional comparisons between isoforms of the sarcoplasmic or endoplasmic reticulum family of calcium pumps. J Biol Chem 267: 14483–9.
- Niebuhr K, Giuriato S, Pedron T, Philpott DJ, Gaits F, Sable J, Sheetz MP, Parsot C, Sansonetti PJ, Payrastre B (2002) Conversion of PtdIns(4,5)P(2) into PtdIns(5)P by the S. flexneri effector IpgD reorganizes host cell morphology. EMBO J21: 5069–5078

- O'Donnell ME, Owen NE (1994) Regulation of ion pumps and carriers in vascular smooth muscle. Physiol Rev 74: 683–721
- Parsot C. (2009) Shigella type III secretion effectors: how, where, when, for what purposes? Current Opinion Microbiology, 12, 110-116.
- Puhar, A., Tronchère, H., Payrastre, B., Tran Van Nhieu, G. & Sansonetti, P. (2013). A Shigella Effector Dampens Inflammation by Regulating Epithelial Release of Danger Signal ATP through Production of the Lipid Mediator PtdIns5P. Immunity, 39, 1121-1131.
- Roos, J., DiGregorio, P., Yeromin, A., Ohlsen, K., Lioudyno, M., Zhang, S., Safrina, O., Kozak, J., Wagner, S., Cahalan, M., Velicelebi, G. & Stauderman, K.. (2005). STIM1, an essential and conserved component of store-operated Ca^{2+} channel function. The Journal of cell biology, 169, 435-445.
- Smedler, E. and Uhlén, P. (2013) Frequency decoding of calcium oscillations. Biochimica et Biophysica Acta, 1840, 964-969.
- Smyth JT, Hwang SY, Tomita T, DeHaven WI, Mercer JC, and Putney JW (2010) Activation and regulation of store-operated calcium entry. J Cell Mol Med 14: 2337–2349.
- Shen WW, Frieden M, Demaurex N (2011) Local cytosolic Ca2+ elevations are required for stromal interaction molecule 1 (STIM1) de-oligomerization and termination of store-operated Ca^{2+} entry. J Biol Chem 286: 36448–59.
- Sun, C., Wacquier, B., Aguilar, D., Carayol, N., Denis, K., Boucherie, S., Valencia-Gallardo, C.,Simsek, C., Erneux, C., Lehman,A., Enninga, J., Arbibe,

L,. Sansonetti, P., Dupont, G., Combette, L. & Tran Van Nhieu, G.. (2017). The Shigella type III effector IpgD recodes Ca2+ signals during invasion of epithelial cells. The EMBO Journal, 1-11.

- Tan, W., Fu, C. and Fu, C. (2007). An anomalous subdiffusion model for calcium spark in cardiac myocytes. Applied physics letters, 91, 283901.
- Tran Van Nhieu, G. and Sansonetti, P. (1999). Mechanism of Shigella entry into epithelial cells. Current Opinion in Microbiology, 2, 51-55.
- Tran Van Nhieu, G., Clair, C., Bruzzone, R., Mesnil, M., Sansonetti, P. and Combettes, L. (2003). Connexin-dependent inter-cellular communication increases invasion and dissemination of Shigellain epithelial cells. Nature Cell Biology, 5, 720-727.
- Tran Van Nhieu, G., Kai Liu, B., Zhang, J., Pierre, F., Prigent, S., Sansonetti, P., Erneux, C., Kuk Kim, J., Suh, P., Dupont, G. and Combettes, L. (2013). Actin-based confinement of calcium responses during Shigella invasion. nature communications, 4, 1-10.
- Weiner A, Mellouk N, Lopez-Montero N, Chang YY, Souque C, Schmitt C, Enninga J (2016) Macropinosomes are key players in early shigella invasion and vacuolar escape in epithelial cells. PLoS Pathog12:e1005602.